Graphical Abstract

Understanding the effect of white matter delays on large scale brain synchrony

Mustafa Şaylı, Stephen Coombes

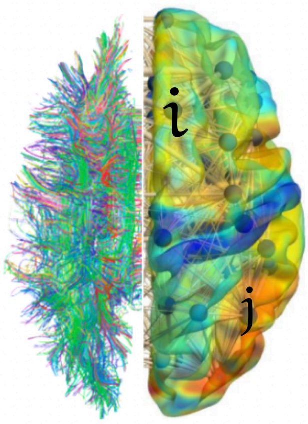

Highlights

Understanding the effect of white matter delays on large scale brain synchrony

Mustafa Şaylı, Stephen Coombes

- A tractable mathematical model of a white matter neural network
- Analysis of the synchronous oscillatory network state (construction and stability)
- Combines techniques from network science, nonsmooth dynamics, and delayed systems

Understanding the effect of white matter delays on large scale brain synchrony

Mustafa Şaylı[a], Stephen Coombes[a,*]

[a] *School of Mathematical Sciences, University of Nottingham, Nottingham, NG7 2RD, UK*

Abstract

The presence of myelin is a powerful structural factor that controls the conduction speed of mammalian axons. It is the combination of local synaptic activity and non-local delayed axonal interactions within the cortex that is believed to be the major source of large-scale brain signals that can be readily observed with modern neuroimaging modalities. Here, we present perspectives from neural mass and network modelling and develop a new set of mathematical tools able to unravel the contributions of space-dependent axonal delays to large-scale spatiotemporal patterning of brain activity. We first analyse a single neuronal population Wilson–Cowan neural mass model with self-feedback and a single delay and show how to construct periodic orbits for a Heaviside firing rate. For this nonsmooth model we perform linear stability analysis by augmenting Floquet theory with saltation operations. Building on this example, we then show how to treat the synchronous oscillatory state in networks of nonsmooth neural masses with multiple and heterogeneous delays. Theoretical predictions for the parameter variations that lead to instabilities of the synchronous network state and the excitation of structured spatio-temporal activity patterns are confirmed with direct numerical simulations.

Keywords: White matter networks, axonal delays, nonsmooth modelling, synchrony
2000 MSC: 34K13, 34K20, 49J52, 92C20, 92B20

1. Introduction

The presence of myelin, a white fatty insulating substance, is a powerful structural factor that controls the conduction speed of mammalian axons. These can extend over the scale of the whole brain and provide the backbone of a communication system for transmitting spikes of electrical activity (action potentials). This allows not only for local interactions, but long-range ones, often between different areas and hemispheres. It is the combination of *local* synaptic activity and *non-local* delayed axonal interactions within the cortex that is believed to be the major source of large-scale brain signals that are seen in electro- and magneto-encephalography (EEG/MEG) recordings [1]. Advances in non-invasive neuroimaging, and specifically diffusion magnetic resonance imaging, now give us a further means to track the locations of myelinated fibre bundles

*Corresponding author
Email addresses: `mustafasaylitr@gmail.com` (Mustafa Şaylı), `stephen.coombes@nottingham.ac.uk` (Stephen Coombes)

and build intricate *white matter networks* that characterise the brain's large-scale topography [2]. This gives a modern view of the human cortex as a dense reciprocally interconnected network of roughly 10^{10} cortico-cortical axonal pathways that make connections within the roughly 3 mm outer layer of the cerebrum. The significance of cortical myeloarchitecture on patterns of functional connectivity (temporal pair-wise correlations of activity) in the human brain is increasingly being recognised, e.g., [3, 4, 5]. Given that axonal delays depend upon tract distances and the speed of action potential propagation, which increases linearly with myelination [6] (and with typical values in the 5 –10 m/s range), then we are faced with understanding a large network with a correspondingly large set of heterogeneous delays. Over large distances, reciprocal coupling of brain nodes generates a significant conduction time (of up to 30 ms in humans) and any variation in the speed of an action potential can be detrimental, since it will disrupt the temporal precision needed for oscillatory coupling and phase-locking [7]. Given the importance of axonal delays in coupling and the potential difficulty in synchronising distant brain areas, it is natural to assume that myelination can play a critical role in resolving this problem. Interestingly, loss of coherence in brain networks is a hallmark of neuropsychiatric disorders such as schizophrenia, see e.g., [8]. One particular pattern of activity that is of fundamental importance in nervous system function and in particular to cognition and the formation of transient functional assemblies is that of *synchrony* [9]. Conduction speeds (and hence delays) in white matter are key to maintaining neural communication and are highly relevant to the *communication through coherence* hypothesis for cognition developed by Fries for brain rhythms in the gamma-band (30 – 90 Hz) [10]. White matter pathways have also been suggested to play a coordinating role for alpha oscillations in the resting visual cortex in a study combining MEG, diffusion tensor imaging, and modelling [11]. Indeed, the modelling of axonal delays in brain models can trace its roots back to the work of Nunez in the 1970s and his development of a brain wave equation (for EEG activity) [12], and recently revisited in [13] in a neural field context incorporating space-dependent axonal delays. Neural fields, typically expressed as integro-differential equations posed on a cortical surface, are simply the continuum counterpart of networks of neural mass models, and such systems are increasingly being adopted to complement neuroimaging studies as exemplified by the activity of the Virtual Brain project [14]. A proto-typical neural mass model is that of Wilson and Cowan, which tracks the activity of an excitatory population of neurons coupled to an inhibitory population [15]. Deco *et al.* have previously used a network of 38 Wilson–Cowan nodes connected according to structural data from the macaque brain with delays determined by assuming a common axonal propagation speed along the connecting fibers based on the 3D Euclidean distance between any 2 connected nodes to show that white matter can play a key role in generating patterns of functional connectivity seen in "resting-state" (default-mode network) [16]. Similar conclusion have been drawn when using human connectome data (with 66 anatomical nodes), albeit for a simplified phase-oscillator Kuramoto network [17, 18]. The latter delayed network model is also able to generate structured amplitude envelopes of band-pass filtered oscillations similar to real resting-state MEG data. More recently, numerical studies of Wilson–Cowan networks with delayed interactions have been shown to be able to generate alpha-band (8 – 12 Hz) networks of phase synchronisation seen in MEG [19], with distant dependent delays (with common axonal propagation speed) providing a best fit to data [20]. All of the above modelling studies rely heavily on numerical simulations to gain insight into spatio-temporal network dynamics. Although the mathematical analysis of steady states in delayed neural networks is relatively well developed, see e.g., [21, 22, 23, 24], that of time periodic oscillations is far less developed with the exception perhaps being the work of Otto *et al.* on synchrony (albeit still requiring the numerical solution of modal differential delay equations) [25], and that of Budzinski *et al.* on the emergence of rotating waves in Kuramoto networks with distance-dependent delays [18]. In this paper we begin to redress this balance by considering a tractable mathematical model of a white matter neural network built from interacting Wilson–Cowan nodes with Heaviside firing rate function. Using techniques from nonsmooth dynamical systems, recent progress in understanding how synchrony can arise in such networks *without* delays has been made in [26]. To handle the non-trivial extension of this work to include axonal delays we build on an approach previously developed to study single delay systems with a threshold nonlinearity [27]. By combining techniques from network science, nonsmooth dynamics, and delayed systems we show how to construct the synchronous oscillatory network state and determine its linear stability.

In section 2 we introduce the dynamics of choice for a single node, namely a Wilson–Cowan model with a Heaviside firing rate and delays between excitatory and inhibitory sub-populations. When all delays are equal, we show how to construct a periodic orbit with two different methods, each with its own merits. The first relies on matrix exponentials (a formulation that proves useful for linear stability) and the second adopts a Fourier series representation (that can accommodate multiple delays). To determine the linear stability of a periodic orbit we augment Floquet theory for smooth systems with a set of saltation operators to handle the nonsmooth behaviour at switching points where the Heaviside firing rate function transitions discontinuously from zero to one. In a regime of co-existing limit cycles we use this to determine that one orbit is stable and the other unstable (with annihilation at a saddle-node of periodic orbits bifurcation). Building on this we then consider circulant networks with a common delay between all nodes in section 3. A modal decomposition in terms of the eigenvectors of the structural connectivity leads to a set of linear stability problems each of which can be handled with the techniques developed in section 2. We use this to predict the onset of a synchronous instability under parameter variation. Direct numerical simulations are used to confirm the bifurcation point and illustrate that the emergent pattern just beyond an instability is well predicted by the unstable eigenvector. The treatment of truly heterogeneous delays is more challenging and we restrict attention to the distant dependent case. A suitable generalisation of the approach in 3 is developed in section 4, and once again theoretical predictions are found to be in excellent agreement with numerical simulations. Finally, in section 5 we review the main results obtained, their relevance to large scale brain modelling, and discuss natural extensions of the work presented.

2. Wilson–Cowan model model with self delays

In the first instance we introduce the Wilson–Cowan model [28] of cortical activity that we subsequently use to describe the dynamics at a node in a brain network model. The Wilson-Cowan model is a ubiquitous model in mathematical neuroscience that has a long and established history of success in describing neuronal population dynamics [29]. The model describes the dynamics of two interacting populations of neurons, one of which is excitatory and the other inhibitory. The equation of the model with the inclusion of fixed communication delay terms between the sub-populations is given by

$$\frac{\mathrm{d}}{\mathrm{d}t}u(t) = -u(t) + F\left(I_u + w^{uu}u(t-\tau_{uu}) - w^{vu}v(t-\tau_{vu})\right), \tag{1}$$

$$\kappa\frac{\mathrm{d}}{\mathrm{d}t}v(t) = -v(t) + F\left(I_v + w^{uv}u(t-\tau_{uv}) - w^{vv}v(t-\tau_{vv})\right). \tag{2}$$

Here, $u(t)$ is a temporal coarse-grained variable describing the proportion of excitatory cells firing per unit time at the instant t. Similarly the variable v represents the activity of an inhibitory population of cells. The constants $w^{\alpha\beta}$, $\alpha, \beta \in \{u, v\}$, describe the weight of all synapses from the αth population to cells of the βth population, $\tau_{\alpha\beta}$ are time delays, I_α represent external inputs (that could be time varying), and κ is a relative time-scale. The nonlinear function F describes the expected proportion of neurons in population α receiving at least threshold excitation per unit time, and is often taken to have a sigmoidal form. Delay differential equations (DDEs), as exemplified by (1)–(2), define a dynamical system with an infinite dimensional phase-space [30] because the history over the delay interval ($[-\max\{\tau_{\alpha\beta}\}, 0]$ for this example) must be specified. Due to this infinite dimensionality, DDEs are difficult to analyse analytically and much is still unknown about their dynamics [30, 31]. A linear stability analysis of fixed points of (1)–(2) can be found in [23] for the case of two distinct delays (where $\tau_{uu} = \tau_{vv}$ and $\tau_{uv} = \tau_{vu}$) and the choice that $F(z) = (1 + \mathrm{e}^{-\beta z})^{-1}$, $\beta > 0$, showing the possibility of delay induced oscillations, and the emergence of chaos with variation in the delays (by the numerical determination of the maximal Lyapunov exponent). Even in the absence of delays, the nonlinearity of a sigmoidal firing rate precludes further analytical progress, except in special cases including that of a Heaviside firing rate function $H(x) = 1$ if $x > 0$ and is zero otherwise. This limiting case of a steep sigmoid has been explored in the Wilson-Cowan model (no delays), e.g., in the work of Harris and Ermentrout [32] for determining formulas for bifurcations of equilibria and that of Coombes *et al.* for the construction and stability of periodic orbits [26]. Indeed, in recent years there has been a growing interest in gaining insight into the behaviour of nonlinear systems with delays. Encouraged by these results, and previous work showing that the treatment of delays and piecewise nonlinearities can oftentimes be tractable [33, 34, 35, 31, 36, 37, 38, 39, 40], we adopt the Heaviside choice throughout the rest of this paper and set $F = H$.

In the absence of delays stable periodic orbits in the Wilson–Cowan model (Heaviside firing rate function) can appear from a (nonsmooth) Hopf bifurcation for $\kappa > \kappa_{\mathrm{Hopf}}$ [32]. With the inclusion of delays it is possible for delay induced oscillations to occur for $\kappa < \kappa_{\mathrm{Hopf}}$, as illustrated in Fig. 1.

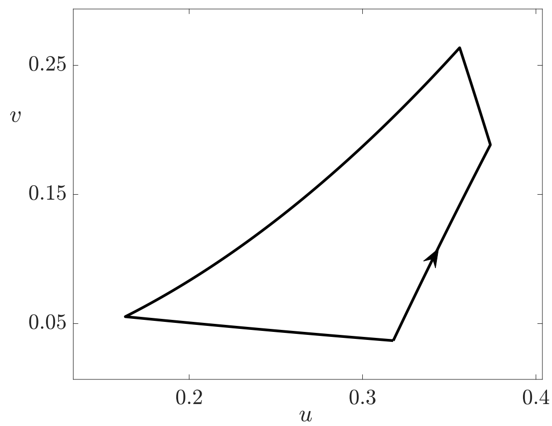

Figure 1: Phase plane for the Wilson-Cowan model with a Heaviside firing rate, showing a delay induced stable periodic orbit. Parameters: $\kappa = 0.5$, $I_u = -0.05$, $I_v = -0.3$, $w^{uu} = 1$, $w^{vu} = 2$, $w^{uv} = 1$, $w^{vv} = 0.25$, with delays $\tau_{uu} = 0.01$, $\tau_{vu} = 0.018$, $\tau_{uv} = 0.012$, and $\tau_{vv} = 0.015$. The switching events occur when $I_u + w^{uu}u(t - \tau_{uu}) - w^{vu}v(t - \tau_{vu}) = 0$ and $I_v + w^{uv}u(t - \tau_{uv}) - w^{vv}v(t - \tau_{vv}) = 0$.

To simplify the analysis and exposition of delay induced oscillations we first consider $\tau_{\alpha\beta} = \tau$, namely we reduce the system to one with a single delay model. We also introduce new variables (U, V) such that $U(t) = I_u + w^{uu}u(t) - w^{vu}v(t)$ and $V(t) = I_v + w^{uv}u(t) - w^{vv}v(t)$ (recognised as the arguments to the firing rate functions in (1)–(2)), as well as the matrices

$$W = \begin{bmatrix} w^{uu} & -w^{vu} \\ w^{uv} & -w^{vv} \end{bmatrix}, \qquad J = \begin{bmatrix} 1 & 0 \\ 0 & 1/\kappa \end{bmatrix} \qquad A = -WJW^{-1}. \tag{3}$$

With these choices (1)-(2) transforms to

$$\frac{\mathrm{d}}{\mathrm{d}t}\begin{bmatrix} U(t) \\ V(t) \end{bmatrix} = A \begin{bmatrix} U(t) - I_u \\ V(t) - I_v \end{bmatrix} + WJ \begin{bmatrix} H(U(t-\tau)) \\ H(V(t-\tau)) \end{bmatrix}. \tag{4}$$

In this representation, switching events occur when the conditions $U(t-\tau) = 0$ or $V(t-\tau) = 0$ hold. In the next subsections we show how to construct periodic solutions of this system and determine their stability.

2.1. Construction of periodic orbits

Away from the switching conditions the dynamics governing the evolution of trajectories is linear, and may be constructed using matrix exponentials. This is because the source term on the right hand side of (4) is piecewise constant, as determined by

$$\begin{bmatrix} H(U(t-\tau)) \\ H(V(t-\tau)) \end{bmatrix} = \begin{cases} [0,0]^\top & \text{if } U(t-\tau) < 0 \text{ and } V(t-\tau) < 0 \\ [1,0]^\top & \text{if } U(t-\tau) > 0 \text{ and } V(t-\tau) < 0 \\ [1,1]^\top & \text{if } U(t-\tau) > 0 \text{ and } V(t-\tau) > 0 \\ [0,1]^\top & \text{if } U(t-\tau) < 0 \text{ and } V(t-\tau) > 0 \end{cases}. \tag{5}$$

The periodic orbit shown in Fig. 2 undertakes each of the switching conditions $U(t-\tau) = 0$ or $V(t-\tau) = 0$ twice, so that the periodic trajectory is naturally decomposed into four separate pieces. On each piece we shall denote the *time-of-flight* for a trajectory to travel from one switching event to another by T_i, $i = 1, \ldots, 4$, so that the period of the orbit is given by $\Delta = \sum_{i=1}^{4} T_i$. As an explicit example of how to construct a trajectory between two switching conditions, consider the region where $U(t-\tau) > 0$ and $V(t-\tau) < 0$. In this case the solution of (4) is given by

$$\begin{bmatrix} U(t) \\ V(t) \end{bmatrix} = \mathrm{e}^{At}\begin{bmatrix} U(0) \\ V(0) \end{bmatrix} + (I_2 - \mathrm{e}^{At})\left[\begin{bmatrix} I_u \\ I_v \end{bmatrix} - A^{-1}WJ\begin{bmatrix} 1 \\ 0 \end{bmatrix}\right], \qquad t \geq 0. \tag{6}$$

It is a simple matter to write down the trajectories in each of the remaining regions of phase space visited by a periodic orbit. We may then use these matrix exponential formulas to *patch* together solutions, setting the origin of time in each region such that *initial* data in one region comes from *final* data from a trajectory in a neighbouring region. We shall denote the periodic orbit by $(\overline{U}, \overline{V})$ such that $(\overline{U}(t), \overline{V}(t)) = (\overline{U}(t+\Delta), \overline{V}(t+\Delta))$. If we consider initial data with $(\overline{U}(0), \overline{V}(0)) = (U_0, V_0)$ then the four times-of-flight and the unknown (U_0, V_0) are determined self-consistently by the six equations $\overline{V}(T_1 - \tau) = 0$, $\overline{U}(T_2 - \tau) = 0$, $\overline{V}(T_3 - \tau) = 0$, $\overline{U}(T_4 - \tau) = 0$, $\overline{U}(T_4) = U_0$, and $\overline{V}(T_4) = V_0$. The numerical solution of this nonlinear algebraic system of equations can be used to construct periodic orbits such as the one shown in Fig. 2, with a fixed pattern of switching consistent with time of flights of the orbit that are larger than the delay durations ($T_i > \tau_{\alpha\beta}$) .

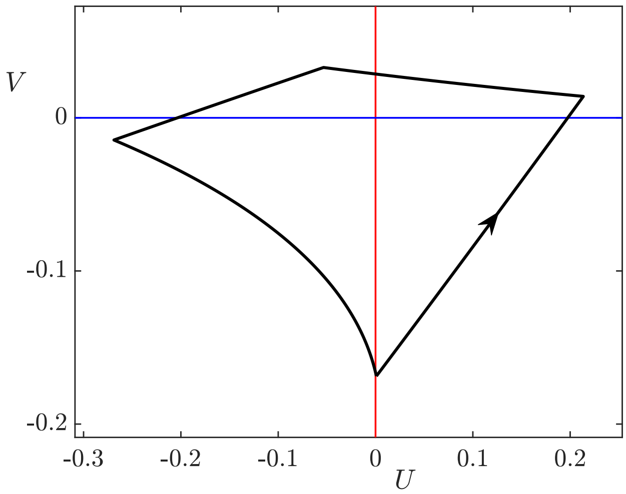

Figure 2: A stable periodic orbit of the model described by (4). Parameters: $\kappa = 0.5$, $I_u = -0.05$, $I_v = -0.3$, $w^{uu} = 1$, $w^{vu} = 2$, $w^{uv} = 1$, $w^{vv} = 0.25$, and delay term $\tau = 0.02$. *Switching* events are prescribed by $U(t-\tau) = 0$ (when the delayed state crosses the red line) and $V(t-\tau) = 0$ (when the delayed state crosses the blue line).

The formulation of trajectories using matrix exponentials is also very useful when considering solutions of the linearised model, as will shall do so shortly for the determination of linear stability of periodic orbits. However, as regards the construction of orbits this approach increases in computational complexity as the number of distinct delays increases, as one now needs to compute state values at more delayed times. Instead it can be more useful to use an alternative Fourier series approach, which is agnostic to the number of delays. To explain this, let us now consider four distinct delays in the Wilson–Cowan model (1)–(2). First we denote unknown times-of-flight of the trajectory by: T_1 in the region $I_u + w^{uu}u(t-\tau_{uu}) - w^{vu}v(t-\tau_{vu}) > 0$ and $I_v + w^{uv}u(t-\tau_{uv}) - w^{vv}v(t-\tau_{vv}) > 0$, T_2 in the region $I_u + w^{uu}u(t-\tau_{uu}) - w^{vu}v(t-\tau_{vu}) < 0$ and $I_v + w^{uv}u(t-\tau_{uv}) - w^{vv}v(t-\tau_{vv}) > 0$, T_3 in the region $I_u + w^{uu}u(t-\tau_{uu}) - w^{vu}v(t-\tau_{vu}) < 0$ and $I_v + w^{uv}u(t-\tau_{uv}) - w^{vv}v(t-\tau_{vv}) < 0$, and T_4 in the region $I_u + w^{uu}u(t-\tau_{uu}) - w^{vu}v(t-\tau_{vu}) > 0$ and $I_v + w^{uv}u(t-\tau_{uv}) - w^{vv}v(t-\tau_{vv}) < 0$. We denote the event times of a periodic orbit by $\Delta_1 = T_1$, $\Delta_2 = T_1 + T_2$, $\Delta_3 = T_1 + T_2 + T_3$ and $\Delta_4 = \Delta$. For a Δ-periodic orbit, the source terms in (1)–(2) are also Δ-periodic and piecewise constant. They can be written as Fourier series such that $H\left(I_u + w^{uu}u(t-\tau_{uu}) - w^{vu}v(t-\tau_{vu})\right) \equiv H^u(t) = \sum_{n\in\mathbb{Z}} H^u_n \mathrm{e}^{2\pi\mathrm{i}nt/\Delta}$ and $H\left(I_v + w^{uv}u(t-\tau_{uv}) - w^{vv}v(t-\tau_{vv})\right) \equiv H^v(t) = \sum_{n\in\mathbb{Z}} H^v_n \mathrm{e}^{2\pi\mathrm{i}nt/\Delta}$. In detail, $H^u(t)$ has the value 1 when $0 < t < \Delta_1$ and $\Delta_3 < t < \Delta$, and 0 when $\Delta_1 < t < \Delta_3$, whilst $H^v(t)$ has the value 1 when $0 < t < \Delta_2$, and 0 when $\Delta_2 < t < \Delta$. The Fourier coefficients $H^{u,v}$ can be computed as

$$H^u_n = \frac{1}{2\pi\mathrm{i}n}\left[1 - \mathrm{e}^{-2\pi\mathrm{i}n\Delta_1/\Delta} + \mathrm{e}^{-2\pi\mathrm{i}n\Delta_3/\Delta}(1 - \mathrm{e}^{-2\pi\mathrm{i}nT_4/\Delta})\right], \tag{7}$$

$$H^v_n = \frac{1}{2\pi\mathrm{i}n}\left[1 - \mathrm{e}^{-2\pi\mathrm{i}n\Delta_2/\Delta}\right]. \tag{8}$$

The Δ-periodic solutions of (1)–(2) can then also be written as Fourier series $(u(t), v(t)) =$

$\sum_{n\in\mathbb{Z}}(u_n, v_n)\mathrm{e}^{2\pi\mathrm{i}nt/\Delta}$, with

$$u_n = \frac{H_n^u}{1 + 2\pi\mathrm{i}n/\Delta}, \qquad v_n = \frac{H_n^v}{1 + \kappa 2\pi\mathrm{i}n/\Delta}. \tag{9}$$

Thus, the coefficients u_n and v_n are expressed in terms of the yet unknowns Δ_i, $i = 1, \ldots, 4$, and these in turn can be found by the numerical solution of the four nonlinear algebraic equations $I_u + w^{uu}u(\Delta_{1,3} - \tau_{uu}) - w^{vu}v(\Delta_{1,3} - \tau_{vu}) = 0$, and $I_v + w^{uv}u(\Delta_{2,4} - \tau_{uv}) - w^{vv}v(\Delta_{2,4} - \tau_{vv}) = 0$. Necessarily, in the numerical approach we must truncate the Fourier series and we do so with the approximation $\sum_{n\in\mathbb{Z}} \to \sum_{n=-N}^{N}$ with $N = 200$. This method of solution construction is illustrated in Fig. 3, and gives seemingly identical results to that of the matrix exponential approach and does not show any obvious Gibbs phenomenon. Let us emphasise that the Fourier approach is far more practical when considering systems with multiple delays.

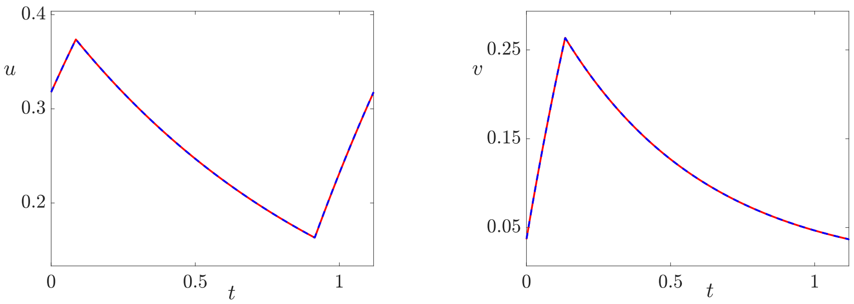

Figure 3: Periodic solution to the Wilson–Cowan model with four distinct delays. The matrix exponential approach is plotted in red and the Fourier series approach in dashed blue (and the two approaches give seemingly identical results). Parameters and delay terms are the same as in Fig. 1. Left: $u(t)$ component. Right: $v(t)$ component.

2.2. *Stability of periodic orbits*

To determine the stability of periodic orbits constructed in section 2.1 we are confronted with analysing perturbations to a nonsmooth and delayed system. In the absence of delays, the extension of Floquet theory to nonsmooth systems with a switching manifold is naturally accommodated with the use of *saltation* operators. In essence these allow for a proper description of how perturbations should be propagated through a switching manifold. For a recent survey of this approach (no delays) we recommend the article by Kong *et al*. [41]. Here, we develop a further extension to treat delays, basing our methodology on ideas developed in [27] for describing instabilities in threshold-diffusion equations with delay. Here, we shall only consider a single delay (with the generalisation to multiple delays to follow later in the paper).

It is convenient to introduce two *indicator* functions $h_1(U, V) = U$ and $h_2(U, V) = V$, respectively, so that the time of events, T, can be defined by $h_i(U(T - \tau), V(T - \tau)) = 0$. Let us introduce the vectors $x(t) = (U(t), V(t))$, $\overline{x}(t) = (\overline{U}(t), \overline{V}(t))$, to represent a perturbed and unperturbed trajectory, and linearise the equations of motion (4) by considering $x(t) = \overline{x}(t) + \delta x(t)$, for small perturbations $\delta x(t) = (\delta U, \delta V)$. In this case (away from switching) we have simply that

$$\frac{\mathrm{d}}{\mathrm{d}t}\delta x = A\,\delta x. \tag{10}$$

Moreover, let us consider the unperturbed trajectory has an event at time $t = T$, prescribed by $h_i(\overline{x}(T-\tau)) = 0$. Similarly we shall consider the perturbed trajectory to switch at a time $\widetilde{T} = T + \delta T$, defined by $h_i(\widetilde{x}(\widetilde{T}-\tau)) = 0$. The indicator function for the perturbed trajectory may be Taylor expanded as:

$$h_i(\widetilde{x}(\widetilde{T}-\tau)) \simeq h_i(\overline{x}(T-\tau)) + \nabla_{x(T-\tau)} h_i(\overline{x}(T-\tau)) \cdot \left[\delta x(T-\tau) + \overline{x}'(T^- - \tau)\delta T\right]. \tag{11}$$

Here we have introduced the notation $x(T^\pm) = \lim_{\epsilon \searrow 0} x(T \pm \epsilon)$, to make sure that derivatives are well defined. Using the fact that $h_i(\overline{x}(T-\tau)) = 0 = h_i(\widetilde{x}(\widetilde{T}-\tau))$ we obtain

$$\nabla_{x(T-\tau)} h_i(\overline{x}(T-\tau)) \cdot \left[\delta x(T-\tau) + \overline{x}'(T^- - \tau)\delta T\right] = 0. \tag{12}$$

Using the result that $\partial h_i(x(t-\tau))/\partial x_j(t-\tau) = \partial x_i(t-\tau)/\partial x_j(t-\tau) = \delta_{i,j}$ (and $\delta_{i,j}$ is a Kronecker delta function), where $(x_1, x_2) = (U, V)$, the above can be re-arranged to give the perturbation in the switching time in terms of the difference between the perturbed and unperturbed trajectories. If the switch occurs at $t = T$ when $V(T-\tau) = 0$ then

$$\delta T = -\frac{\delta V(T-\tau)}{\overline{V}'(T^- - \tau)}, \tag{13}$$

and if the switch occurs at $t = T$ when $U(T-\tau) = 0$ then

$$\delta T = -\frac{\delta U(T-\tau)}{\overline{U}'(T^- - \tau)}. \tag{14}$$

We now construct the deviation between the two trajectories at the perturbed switching time as

$$\delta x(T+\delta T) = \widetilde{x}(T+\delta T) - \overline{x}(T+\delta T) \simeq \delta x(T) + [\widetilde{x}'(T) - \overline{x}'(T)]\delta T. \tag{15}$$

If $\delta T > 0$ then the unperturbed trajectory will already have switched, in which case the two trajectories are on either side of the switching manifold. A similar argument holds for $\delta T < 0$. Thus we may write

$$\delta x(T+\delta T) \simeq \delta x(T) + \left[\overline{x}'(T^-) - \overline{x}'(T^+)\right]\delta T. \tag{16}$$

Let us first consider the switch to occur at $t = T$ when $V(T-\tau) = 0$ holds, so that δT is given by (13). In this case (16) gives $\delta x(T+\delta T) = \delta x(T) + K_a(T)\delta x(T-\tau)$ with

$$K_a(T) = \begin{bmatrix} 0 & (\overline{U}'(T^+) - \overline{U}'(T^-))/\overline{V}'(T^- - \tau) \\ 0 & (\overline{V}'(T^+) - \overline{V}'(T^-))/\overline{V}'(T^- - \tau) \end{bmatrix}. \tag{17}$$

If the switch occurs at $t = T$ when $U(T-\tau) = 0$ holds, then a similar calculation gives $\delta x(T + \delta T) = \delta x(T) + K_b(T)\delta x(T-\tau)$, with

$$K_b(T) = \begin{bmatrix} (\overline{U}'(T^+) - \overline{U}'(T^-))/\overline{U}'(T^- - \tau) & 0 \\ (\overline{V}'(T^+) - \overline{V}'(T^-))/\overline{U}'(T^- - \tau) & 0 \end{bmatrix}. \tag{18}$$

Hence due to the discontinuous change in the vector fields there are discontinuous changes during the evolution of perturbation at the switching times, i.e., $\delta x(T^+) = \delta x(T^-) + K_{a,b}(T)\delta x(T-\tau)$. Here $K_{a,b}(T)\delta x(T-\tau)$ describe the sudden changes (jumps) in the perturbation at an event time

$t = T$. Note that this jump depends upon the value of the perturbation in the *delayed* past. In Appendix A we show that the saltation operators $K_{a,b}(\Delta_i) \equiv K_i$ can be written explicitly as

$$K_1 = \frac{1}{\overline{V}'(\Delta_1^- - \tau)} WJ \begin{bmatrix} 0 & 0 \\ 0 & 1 \end{bmatrix}, \qquad K_2 = \frac{-1}{\overline{U}'(\Delta_2^- - \tau)} WJ \begin{bmatrix} 1 & 0 \\ 0 & 0 \end{bmatrix},$$
$$K_3 = \frac{-1}{\overline{V}'(\Delta_3^- - \tau)} WJ \begin{bmatrix} 0 & 0 \\ 0 & 1 \end{bmatrix}, \qquad K_4 = \frac{1}{\overline{U}'(\Delta_4^- - \tau)} WJ \begin{bmatrix} 1 & 0 \\ 0 & 0 \end{bmatrix}. \tag{19}$$

Returning to equation (10), and following standard practice for Floquet theory, we write the solution away from the switches in the form $\delta x(t) = e^{\lambda t} z(t)$, where $\lambda \in \mathbb{C}$ are Floquet exponents and $z(t)$ is $\Delta-$periodic. Thus, away from switches $z(t)$ satisfies $z' = (A - \lambda I_2)z$, with matrix exponential solution $z(t) = e^{(A-\lambda I_2)t} z(0)$ for $t > 0$. Remembering that at switching times $t = \Delta_j$, $j = 1, \ldots, 4$, $z(t)$ will undergo sudden changes, as described above, then we may write $z(\Delta_j^+) = z(\Delta_j^-) + e^{-\lambda\tau} K_j z(\Delta_j - \tau)$. By combining the linear evolution between events and jump conditions (at the switches), we can compute $z(t)$ over one period $[0, \Delta]$ as

$$z(t) = \begin{cases} z(0^-), \quad t = 0, \\ \zeta(t)[z(0^-) + S_4(0)], \quad 0 < t \le \Delta_1, \\ \zeta(t - \Delta_1)[S_1(\Delta_1) + \zeta(\Delta_1)[z(0^-) + S_4(0)]], \quad \Delta_1 < t \le \Delta_2, \\ \zeta(t - \Delta_2)[S_2(\Delta_2) + \zeta(T_2)[S_1(\Delta_1) + \zeta(\Delta_1)[z(0^-) + S_4(0)]]], \quad \Delta_2 < t \le \Delta_3, \\ \zeta(t - \Delta_3)[S_3(\Delta_3) + \zeta(T_3)[S_2(\Delta_2) + \zeta(T_2)[S_1(\Delta_1) + \zeta(\Delta_1)[z(0^-) + S_4(0)]]]], \Delta_3 < t \le \Delta, \end{cases} \tag{20}$$

Here, $\zeta(t) = e^{(A-\lambda I_2)t} H(t)$ and $S_{1,\ldots,4}(\Delta_i)$ denote the various *jumps* in $z(t)$ illustrated in Fig. 4 given by:

$$\begin{aligned} S_1(\Delta_1) &= e^{-\lambda\tau} K_1 z(\Delta_1 - \tau), \quad S_2(\Delta_2) = e^{-\lambda\tau} K_2 z(\Delta_2 - \tau), \\ S_3(\Delta_3) &= e^{-\lambda\tau} K_3 z(\Delta_3 - \tau), \quad S_4(\Delta_4) = e^{-\lambda\tau} K_4 z(\Delta_4 - \tau). \end{aligned} \tag{21}$$

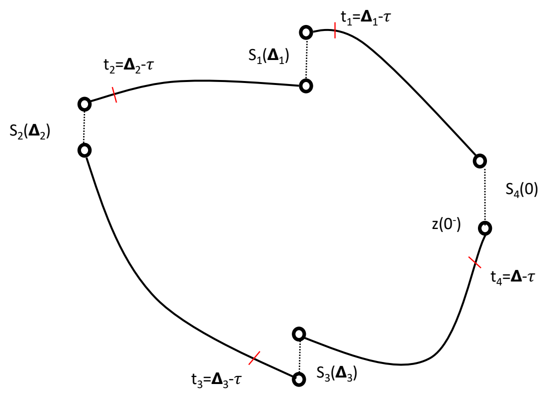

Figure 4: An illustration of the shape of the $\Delta-$periodic $z(t)$ and the dependence of jumps at times Δ_i on the delayed state $z(\Delta_i - \tau)$.

The formula for $z(t)$ given by (20) is only implicit in the sense that it depends on the as yet unknowns $z(\Delta_i - \tau)$ occurring in the terms S_i. However, these can be determined self consistently by considering the times $t = t_i$, where $t_i = \Delta_i - \tau$, and remembering that periodicity of $z(t)$ requires $z(0^-) = z(\Delta)$. The evaluation of $z(t)$ at the these four times results in four equations for the unknown planar amplitudes $(z(t_1)\ z(t_2)\ z(t_3)\ z(t_4))$ which takes the form $\mathscr{U}(\lambda)[z(t_1)\ z(t_2)\ z(t_3)\ z(t_4)]^\top = 0$ where $\mathscr{U}(\lambda)$ is given by

$$\mathscr{U}(\lambda) = \begin{bmatrix} \mathscr{V}_1(t_1,\lambda) - I_2 & \mathscr{V}_3(t_1,\lambda) & \mathscr{V}_5(t_1,\lambda) & \mathscr{V}_7(t_1,\lambda) \\ \mathscr{V}_2(t_2,\lambda) + \mathscr{V}_1(t_2,\lambda) & \mathscr{V}_3(t_2,\lambda) - I_2 & \mathscr{V}_5(t_2,\lambda) & \mathscr{V}_7(t_2,\lambda) \\ \mathscr{V}_2(t_3,\lambda) + \mathscr{V}_1(t_3,\lambda) & \mathscr{V}_4(t_3,\lambda) + \mathscr{V}_3(t_3,\lambda) & \mathscr{V}_5(t_3,\lambda) - I_2 & \mathscr{V}_7(t_3,\lambda) \\ \mathscr{V}_2(t_4,\lambda) + \mathscr{V}_1(t_4,\lambda) & \mathscr{V}_4(t_4,\lambda) + \mathscr{V}_3(t_4,\lambda) & \mathscr{V}_6(t_4,\lambda) + \mathscr{V}_5(t_4,\lambda) & \mathscr{V}_7(t_4,\lambda) - I_2 \end{bmatrix}, \tag{22}$$

with

$$\begin{aligned} &\mathscr{V}_1(t,\lambda) = p(t)\zeta(\Delta - \Delta_1)K_1, \quad \mathscr{V}_2(t,\lambda) = p(t)(I_2 - \zeta(\Delta))\zeta(\Delta_1)^{-1}K_1, \\ &\mathscr{V}_3(t,\lambda) = p(t)\zeta(\Delta - \Delta_2)K_2, \quad \mathscr{V}_5(t,\lambda) = p(t)\zeta(\Delta - \Delta_3)K_3, \\ &\mathscr{V}_4(t,\lambda) = p(t)(I_2 - \zeta(\Delta))\zeta(\Delta_1)^{-1}\zeta(\Delta_2 - \Delta_1)^{-1}K_2, \quad \mathscr{V}_7(t,\lambda) = p(t)K_4, \\ &\mathscr{V}_6(t,\lambda) = p(t)(I_2 - \zeta(\Delta))\zeta(\Delta_1)^{-1}\zeta(\Delta_2 - \Delta_1)^{-1}\zeta(\Delta_3 - \Delta_2)^{-1}K_3, \end{aligned} \tag{23}$$

and $p(t) = \zeta(t)\mathrm{e}^{-\lambda\tau}[I_2 - \zeta(\Delta)]^{-1}$.

Demanding a non-trivial solution of this system gives an equation for the Floquet exponents λ in the form $\varepsilon(\lambda) \equiv \det(\mathscr{U}_\lambda) = 0$. Solutions will be linearly stable provided $\mathrm{Re}\,\lambda < 0$. To compute the zeros of $\varepsilon(\lambda)$ it is practical to first decompose λ as $\lambda \equiv \nu + \mathrm{i}\omega$. The pair (ν, ω) may then be found by the simultaneous solution of $\varepsilon_\mathrm{R}(\nu, \omega) \equiv 0$ and $\varepsilon_\mathrm{I}(\nu, \omega) \equiv 0$, where $\varepsilon_\mathrm{R}(\nu, \omega) = \mathrm{Re}\,\varepsilon(\nu+\mathrm{i}\omega)$ and $\varepsilon_\mathrm{I}(\nu, \omega) = \mathrm{Im}\,\varepsilon(\nu+\mathrm{i}\omega)$. Hence an examination of a plot of the zero contours of $\varepsilon_{\mathrm{I,R}}$ can be used to reveal the point spectrum with Floquet exponents occurring where the two contours intersect. For the periodic orbits shown in Fig. 5, plots obtained in this fashion are shown in Fig. 6. For the perturbation in the same direction with the periodic orbit, we see one exponent with $\lambda = 0$ as expected (from time translation invariance), and some others just slightly to the left or right of the imaginary axis. For the green solution shown in Fig. 5, no exponents are ever found in the right hand complex plane, and so this periodic orbits is stable but for the black dotted orbit there are exponents on the right hand complex plane, therefore it is unstable.

3. Nonsmooth Wilson-Cowan networks with homogeneous delay

The machinery of section 2, for the construction and stability of periodic orbits, can be readily extended to treat networks of N interacting Wilson–Cowan nodes in larger networks. Before describing how to do this for heterogeneous delays, we first given an exposé for networks with a common delay to set the scene for dealing with the more general case of heterogeneous delays. Thus, we consider a network of Wilson-Cowan nodes given by

$$\frac{\mathrm{d}}{\mathrm{d}t}u_i(t) = -u_i(t) + H\left(I_u + \sum_{j=1}^{N} \mathcal{W}_{ij}^{uu} u_j(t-\tau) - \sum_{j=1}^{N} \mathcal{W}_{ij}^{vu} v_j(t-\tau)\right), \tag{24}$$

$$\kappa\frac{\mathrm{d}}{\mathrm{d}t}v_i(t) = -v_i(t) + H\left(I_v + \sum_{j=1}^{N} \mathcal{W}_{ij}^{uv} u_j(t-\tau) - \sum_{j=1}^{N} \mathcal{W}_{ij}^{vv} v_j(t-\tau)\right), \qquad i = 1, \ldots, N, \tag{25}$$

where τ represents a homogeneous delay. It is convenient to introduce a vector notation with $X = (u_1, v_1, u_2, v_2, \ldots, u_N, v_N) \in \mathbb{R}^{2N}$ and consider a change of variables $Y(t) = \mathcal{W}X(t) + C$,

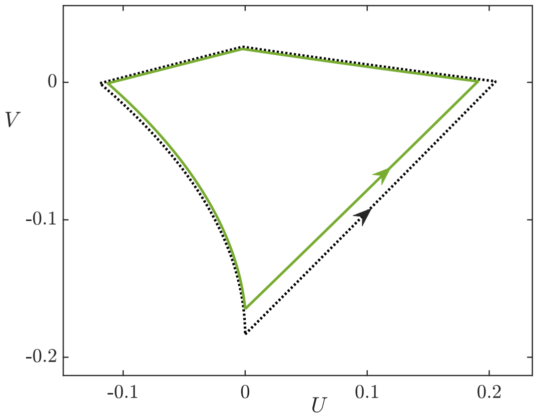

Figure 5: Stable (green) and unstable (dotted black) periodic orbits of the model described by (4). Parameters: $\kappa = 0.6$, $I_u = -0.05$, $I_v = -0.3$, $w^{uu} = 1$, $w^{vu} = 2$, $w^{uv} = 1$, $w^{vv} = 0.25$, and delay term $\tau = 0.001$.

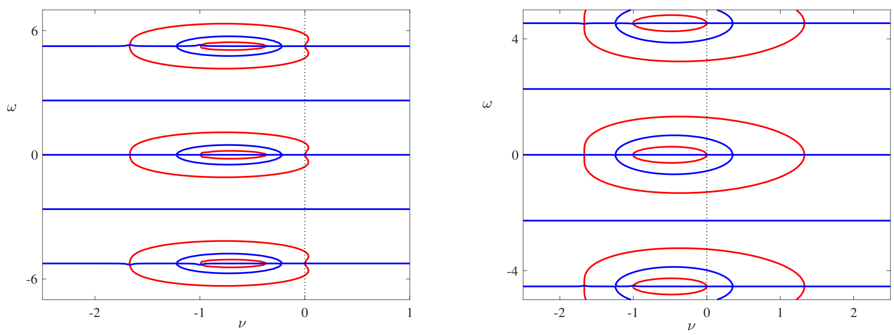

Figure 6: Floquet exponents as zeros of a complex analytic function $\mathcal{E}(\lambda)$. Floquet exponents occur where the zero contours of $\mathcal{E}_R$ and $\mathcal{E}_I$ (red and blue lines) intersect. Note the presence of a zero exponent, as expected for perturbations tangential to the periodic orbit. Left: spectrum for the orbit coloured in green in Fig. 5. Since there are no zeros of $\mathcal{E}(\lambda)$ in the right hand complex plane, the solution is linearly stable. Right: spectrum for the orbit coloured in black (dotted) in Fig. 5. The presence of zeros of $\mathcal{E}(\lambda)$ in the right hand complex plane show that the solution is linearly unstable.

where $C = \mathbf{1}_N \otimes (I_u, I_v)$, and

$$\mathcal{W} = \mathcal{W}^{uu} \otimes \begin{bmatrix} 1 & 0 \\ 0 & 0 \end{bmatrix} - \mathcal{W}^{vu} \otimes \begin{bmatrix} 0 & 1 \\ 0 & 0 \end{bmatrix} + \mathcal{W}^{uv} \otimes \begin{bmatrix} 0 & 0 \\ 1 & 0 \end{bmatrix} - \mathcal{W}^{vv} \otimes \begin{bmatrix} 0 & 0 \\ 0 & 1 \end{bmatrix}. \tag{26}$$

Here, $\otimes$ denotes the tensor (Kronecker) product and $\mathbf{1}_N$ is an N-dimensional vector with all entries equal to 1. This means that the switching manifolds can be succinctly described by $h_i(Y(t-\tau)) = Y_i(t-\tau) = 0$ and the dynamics takes the form

$$\frac{\mathrm{d}}{\mathrm{d}t} Y(t) = \mathcal{A}(Y(t) - C) + \mathcal{W}\mathcal{J}H(Y(t-\tau)), \tag{27}$$

where

$$\mathcal{J} = I_N \otimes J, \qquad \mathcal{A} = -\mathcal{W}\mathcal{J}\mathcal{W}^{-1}. \tag{28}$$

For the rest of the paper we shall focus on *synchronous solutions* (and the methodologies we develop here can be further adapted to treat other phase-locked and cluster states). By synchrony, we mean periodic solutions of the form $(u_i(t), v_i(t)) = (u(t), v(t))$ for all $i = 1, \ldots, N$. These are guaranteed to exist for certain forms of coupling, including ones with the row sum constraints $\sum_{j=1}^{N} \mathcal{W}_{ij}^{uu} = w^{uu}$, $\sum_{j=1}^{N} \mathcal{W}_{ij}^{vu} = w^{vu}$, $\sum_{j=1}^{N} \mathcal{W}_{ij}^{uv} = w^{uv}$, and $\sum_{j=1}^{N} \mathcal{W}_{ij}^{vv} = w^{vv}$ for all i. In this case the network supports a periodic solution $(u_i(t), v_i(t)) = (u(t), v(t))$ if the dynamics for a single Wilson–Cowan node also admits a periodic solution such that $(u(t), v(t)$ is a periodic solution of (1)–(2). If we denote the synchronous solution by $\overline{Y}(t) = (\overline{U}(t), \overline{V}(t), \overline{U}(t), \overline{V}(t), \ldots, \overline{U}(t), \overline{V}(t))$ and consider small perturbations such that $Y = \overline{Y} + \delta Y$, then these evolve according to

$$\frac{\mathrm{d}}{\mathrm{d}t}\delta Y(t) = \mathcal{A}\delta Y(t) + \mathcal{W}\mathcal{J}\mathrm{D}H(\overline{Y}(t-\tau))\delta Y(t-\tau), \tag{29}$$

where $\mathrm{D}H(\overline{Y}(t-\tau))$ represents the Jacobian obtained along the orbit. (Remembering that H is not differentiable, we shall use the distributional approach and write $H'(x) = \delta(x)$ where $\delta(x)$ is a Dirac delta function).

Given the constraints on the matrices $\mathcal{W}^{\alpha\beta}$, with $\alpha, \beta \in \{u, v\}$ it is natural to take these to be circulant matrices with $\mathcal{W}_{ij}^{\alpha\beta} = \mathcal{W}_{|i-j|}^{\alpha\beta}$. In this case the normalised eigenvectors of $\mathcal{W}^{\alpha\beta}$ are given by $e_q = (1, \omega_q, \omega_q^2, \ldots, w_q^{N-1})/\sqrt{N}$, where $q = 0, \ldots, N-1$, and $\omega_q = \exp(2\pi \mathrm{i} q/N)$ are the Nth roots of unity. The corresponding eigenvalues are given by $\nu^{\alpha\beta} = \nu^{\alpha\beta}(q)$ where

$$\nu^{\alpha\beta}(q) = \sum_{j=0}^{N-1} \mathcal{W}_j^{\alpha\beta}\omega_q^j. \tag{30}$$

If we introduce the matrix of eigenvectors $P = [e_0 \; e_1 \; \ldots \; e_{N-1}]$, then we have that

$$(P \otimes I_2)^{-1}\mathcal{W}(P \otimes I_2) = \mathrm{diag}(\Lambda(0), \Lambda(1), \ldots, \Lambda(N-1)) \equiv \Lambda, \tag{31}$$

where $\Lambda^{\alpha\beta} = \mathrm{diag}(\nu^{\alpha\beta}(0), \nu^{\alpha\beta}(0), \ldots, \nu^{\alpha\beta}(N-1))$, and

$$\Lambda(q) = \begin{bmatrix} \nu^{uu}(q) & -\nu^{vu}(q) \\ \nu^{uv}(q) & -\nu^{vv}(q) \end{bmatrix}, \qquad q = 0, 1, \ldots, N-1. \tag{32}$$

Moreover, in the above notation $(P \otimes I_2)^{-1}\mathcal{A}(P \otimes I_2) = \Lambda(I_N \otimes J)\Lambda^{-1}$.

If we now consider perturbations of the form $\delta Z(t) = (P \otimes I_2)^{-1}\delta Y(t)$ then from (29) we find that

$$\frac{\mathrm{d}}{\mathrm{d}t}\delta Z(t) = -\Lambda(I_N \otimes J)\Lambda^{-1}\delta Z(t) + \Lambda(I_N \otimes J\mathrm{D}H)\delta Z(t-\tau), \tag{33}$$

where $\mathrm{D}H \in \mathbb{R}^{2\times 2}$ now represents the Jacobian of $(H(\overline{U}(t-\tau)), H(\overline{V}(t-\tau)))$. We see that (33) has block structure where the dynamics in each of N 2×2 block is given by

$$\frac{\mathrm{d}}{\mathrm{d}t}\xi_q(t) = A(q)\xi_q(t) + \Lambda(q)J\mathrm{D}H\xi_q(t-\tau), \qquad q = 0, 1, \ldots, N-1, \tag{34}$$

where $\xi_q \in \mathbb{C}^2$ and $A(q) = -\Lambda(q)J\Lambda^{-1}(q)$. We note that between the events $\mathrm{D}H \equiv 0$ therefore this system evolves according to $\xi_q'(t) = A(q)\xi_q(t)$. More generally, the formal solution to the system (34) can be written as

$$\xi_q(t) = \mathrm{e}^{A(q)(t-t_0)}\xi_q(t_0) + \int_{t_0}^{t} \mathrm{e}^{A(q)(t-s)}\Lambda(q)J\begin{bmatrix}\delta(\overline{U}(s-\tau)) & 0 \\ 0 & \delta(\overline{V}(s-\tau))\end{bmatrix}\xi_q(s-\tau)\mathrm{d}s, \tag{35}$$

for $t > t_0$. We note that an event occurs at $t = T$ whenever $\overline{U}(T-\tau) = 0$ or $\overline{V}(T-\tau) = 0$, and that the only contributions from the delta functions in (35) are from switching events. Let us first consider the switching event defined by $\overline{U}(T-\tau) = 0$. In this case, across the time of an event we have that

$$\xi_q(T^+) = \xi_q(T^-) + \lim_{\epsilon\searrow 0}\int_{T-\epsilon}^{T+\epsilon} \mathrm{e}^{A(q)(T-s)}\Lambda(q)J\begin{bmatrix}\delta(\overline{U}(s-\tau)) & 0 \\ 0 & 0\end{bmatrix}\xi_q(s-\tau)\mathrm{d}s. \tag{36}$$

Using a change of variable we can transform (36) to

$$\begin{aligned}\xi_q(T^+) &= \xi_q(T^-) \\ &+ \lim_{\epsilon\searrow 0}\int_{\overline{U}(T-\tau-\epsilon)}^{\overline{U}(T-\tau+\epsilon)} \mathrm{e}^{A(q)(T-(\overline{U}^{-1}(z)+\tau))}\Lambda(q)J\begin{bmatrix}\delta(z) & 0 \\ 0 & 0\end{bmatrix}\xi_q(\overline{U}^{-1}(z))\frac{\mathrm{d}z}{|\overline{U}'(\overline{U}^{-1}(z))|},\end{aligned} \tag{37}$$

to obtain

$$\xi_q(T^+) = \xi_q(T^-) + \Lambda(q)J\begin{bmatrix}\frac{1}{|\overline{U}'(T-\tau)|} & 0 \\ 0 & 0\end{bmatrix}\xi_q(T-\tau). \tag{38}$$

Similarly, for a switching event defined by $\overline{V}(T-\tau) = 0$, we have that

$$\xi_q(T^+) = \xi_q(T^-) + \Lambda(q)J\begin{bmatrix}0 & 0 \\ 0 & \frac{1}{|\overline{V}'(T-\tau)|}\end{bmatrix}\xi_q(T-\tau). \tag{39}$$

Hence, the forms of (38) and (39) capture the jumps in perturbations around a synchronous orbit, and in turn these can be represented using saltation operators indexed by q. These are the natural generalisations of (19) to networks, and take the explicit form

$$\begin{aligned} K_1(q) &= \frac{1}{\overline{V}'(\Delta_1-\tau)}\Lambda(q)J\begin{bmatrix}0 & 0 \\ 0 & 1\end{bmatrix}, \quad & K_2(q) &= \frac{-1}{\overline{U}'(\Delta_2-\tau)}\Lambda(q)J\begin{bmatrix}1 & 0 \\ 0 & 0\end{bmatrix}, \\ K_3(q) &= \frac{-1}{\overline{V}'(\Delta_3-\tau)}\Lambda(q)J\begin{bmatrix}0 & 0 \\ 0 & 1\end{bmatrix}, \quad & K_4(q) &= \frac{1}{\overline{U}'(\Delta_4-\tau)}\Lambda(q)J\begin{bmatrix}1 & 0 \\ 0 & 0\end{bmatrix}. \end{aligned} \tag{40}$$

We note that for $q = 0$ the variational problem is identical to that for an isolated node since $\Lambda(0) = W$ (using $v^{\alpha\beta}(0) = \sum_{j=0}^{N-1} \mathcal{W}_j^{\alpha\beta} = w^{\alpha\beta}$), and $A(0) = A$. In addition to this, when $q = 0$ one can check that $K_i(0) = K_i$ as given by (19).

In summary, we see that the variational equations for the network are identical to that for a single Wilson-Cowan unit with W replaced by $\Lambda(q)$ subject to block dependent saltation (described using $K_i(q)$). Thus, to determine the stability of the synchronous state we only have to consider a set of N two dimensional variational problems. Each of these can be solved using the method described in Section 2.2, originally developed for the study of a single isolated node. Explicitly, for each q, we introduce $\xi_q(t) = \mathrm{e}^{\lambda t}z_q(t)$, where $\lambda \in \mathbb{C}$ (Floquet exponents) and $z_q(t)$ are $\Delta-$periodic. Then away from the switches, each Δ-periodic $z_q(t)$ evolves according to

$$z_q' = (A(q) - \lambda I_2)z_q. \tag{41}$$

Across a switch

$$z_q(\Delta_j^+) = z_q(\Delta_j^-) + \mathrm{e}^{-\lambda\tau} K_j(q) z(\Delta_j - \tau). \tag{42}$$

Generalising the treatment in section 2.2 gives rise to a set of Floquet problems indexed by $q = 0, \dots, N-1$, with the Floquet exponents satisfying $\mathcal{E}_q(\lambda) = 0$, where $\mathcal{E}_q(\lambda)$ is obtained from $\mathcal{E}(\lambda)$ under the replacement $K_j \to K_j(q)$, $\zeta(t) \to \zeta_q(t) = \mathrm{e}^{(A(q)-\lambda I_2)t} H(t)$ and $p(t) \to p_q(t) = \zeta_q(t)\mathrm{e}^{-\lambda\tau}[I_2 - \zeta_q(\Delta)]^{-1}$.

Thus if a periodic orbit of an isolated Wilson-Cowan node is linearly stable (corresponding to $q = 0$) then the synchronous network solution will be linearly stable provided all solutions of $\mathcal{E}_q(\lambda) = 0$ have $\mathrm{Re}\,\lambda < 0$ for all $q = 1, \dots, N-1$.

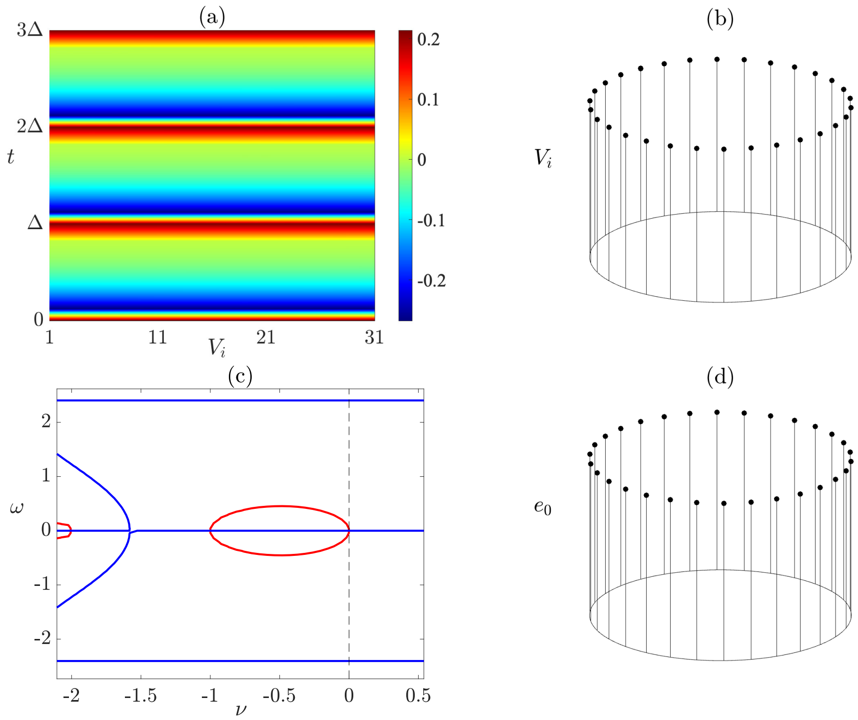

Figure 7: Dynamics of a Wilson–Cowan ring network with $N = 31$ nodes and homogeneous delays in a parameter regime where the synchronous solution is predicted to be linearly stable. (a) Space time plot of the network activity of $V_i(t)$ from direct simulation. (b) A representation of V_i at a fixed time across the network. (c) The Floquet exponents coincide with the intersections of the zero contours of $\mathcal{E}_q^{\mathrm{I,R}}(\lambda)$ (red and blue lines). These have maximum real part for $q = 0$ (and the remaining zeros of $\mathcal{E}_q(\lambda)$ for $q = 1, \dots, 30$ occur in the left hand complex plane). Since $\mathcal{E}_q(\lambda)$ has no zeros in the right hand complex plane the synchronous solution is linearly stable. (d) Shape of the eigenvector e_0 associated with $q = 0$. Parameters: $\mu = 0.239$, $\tau = 0.02$, and other parameters as in Fig. 2.

3.1. *Instabilities in a ring network: homogeneous delays*

By way of illustration of the above theory let us consider a network of Wilson–Cowan nodes arranged on a ring with an odd number of nodes. Introducing a distance between nodes indexed

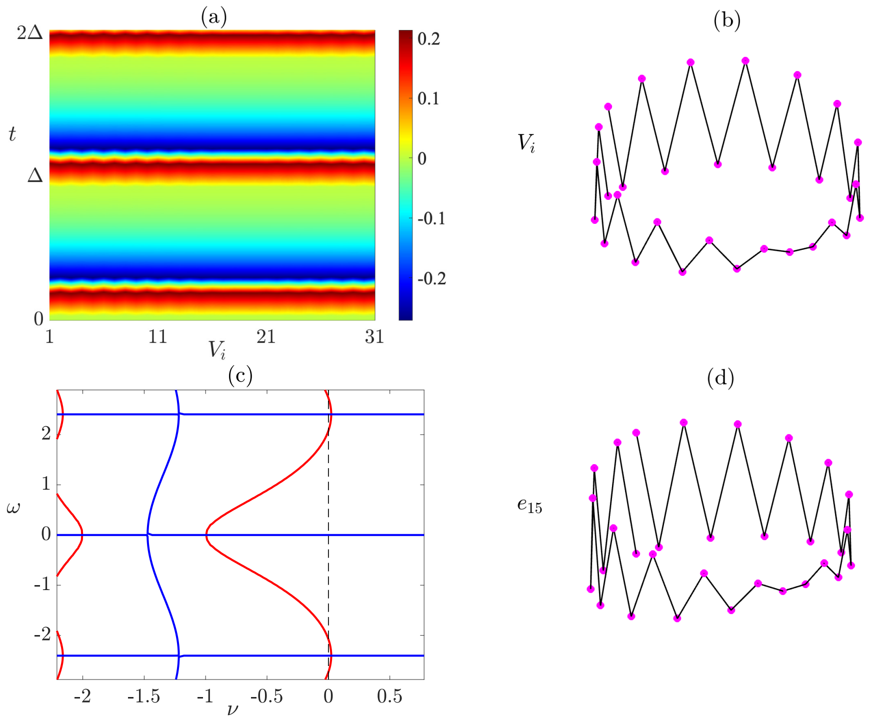

Figure 8: Dynamics of a Wilson–Cowan ring network with $N = 31$ nodes and homogeneous delays in a parameter regime where the synchronous solution is predicted to be linearly unstable. (a) Space time plot of the network activity of $V_i(t)$ from direct simulation. (b) A representation of V_i at a fixed time across the network. (c) The Floquet exponents coincide with the intersections of the zero contours of $\varepsilon_q^{\mathrm{I,R}}(\lambda)$ (red and blue lines). Here $q = 15$, and for all other values of q the zeros of $\varepsilon_q(\lambda)$ occurs in the left hand complex plane. The presence of zeros of $\varepsilon^{15}(\lambda)$ in the right hand complex plane show that the synchronous solution is linearly unstable. (d) A plot of the shape of the corresponding eigenvector e_{15} associated with $q = 15$. The spatial pattern of the network state is well predicted by shape of e_{15}. Parameters: $\mu = 0.241$, $\tau = 0.02$, and other parameters as in Fig. 2.

by i and j as $\mathrm{dist}(i, j) = \min(|i - j|, N - |i - j|)$, we can define a set of exponentially decaying connectivity matrices, with spatial scale μ, according to

$$\mathcal{W}_{ij}^{\alpha\beta} = w^{\alpha\beta} \frac{\mathrm{e}^{-\mathrm{dist}(i,j)/\mu}}{\sum_{j=0}^{N-1} \mathrm{e}^{-\mathrm{dist}(0,j)/\mu}}. \tag{43}$$

In the following we use the preceding theoretical work to determine network instabilities of the synchronous state under variation in μ, and confirm the predictions of patterning beyond an instability against direct numerical simulations. Analogous to the method in section 2.2 we introduce the functions $\varepsilon_q^{\mathrm{R}}(\nu, \omega) = \mathrm{Re}\, \varepsilon_q(\nu + \mathrm{i}\omega)$ and $\varepsilon_q^{\mathrm{I}}(\nu, \omega) = \mathrm{Im}\, \varepsilon_q(\nu + \mathrm{i}\omega)$, and find Floquet exponents as intersections of the zero contours of $\varepsilon_q^{\mathrm{I,R}}$.

For a fixed network size, fixed delay, and all other parameters fixed it is possible for an instability of the synchronous state to occur with an increase in μ through a critical value μ_c. For the parameters of Fig. 7 and Fig. 8 we find $\mu_c \simeq 0.24$. The former figure illustrates network behaviour for $\mu < \mu_c$ and the latter for $\mu > \mu_c$. In both cases the theoretical predictions for stability/instability of the synchronous solution agree with the results from direct numerical simulations. Moreover, just beyond an instability the shape of the unstable eigenmode is shown to be an excellent predictor for the spatial pattern of activity. For larger values of μ (so that we are further beyond the bifurcation point) it is possible for many different modes (multiple distinct values of q) to become unstable, as illustrated in Fig. 9. In this case, the predictions of network pattern states from linear stability will break down (as modes may mix nonlinearly), though direct numerical simulations can be useful for probing emergent behaviour. Doing so shows the possibility of complex locked patterns, as illustrated in Fig. 10. The correlations between time-series at distinct nodes will then give rise to non-trivial patterns of functional connectivity.

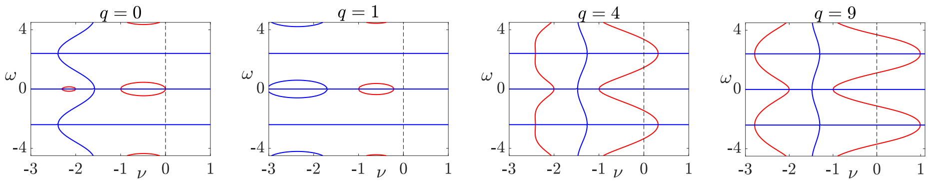

Figure 9: The Floquet exponents for a Wilson–Cowan ring network with $N = 31$ nodes and homogeneous delays (as intersections of the zero contours of $\mathcal{E}_q^{\mathrm{I,R}}(\lambda)$, given by the red and blue lines). Far from bifurcation it is possible that many different modes (multiple distinct values of q) can become unstable. Here, we see that modes with $q = 4$ and $q = 9$ are simultaneously unstable. Parameters: $\mu = 0.45$, and other parameters as in Fig. 8.

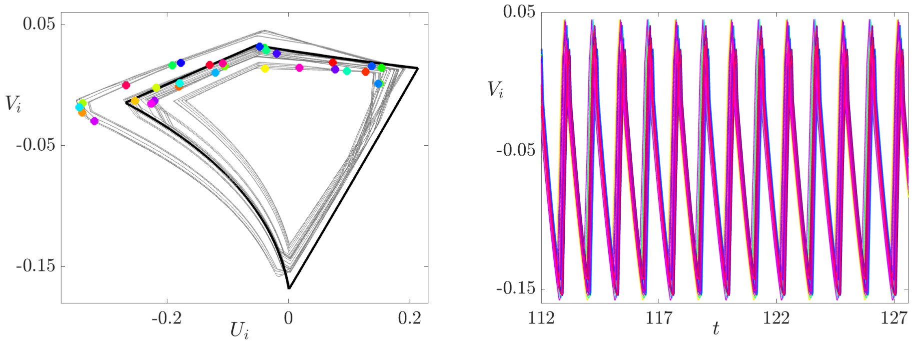

Figure 10: Dynamics of a Wilson–Cowan ring network with $N = 31$ nodes and homogeneous delays in a parameter regime far beyond bifurcation where multiple Floquet exponents have positive real part. Left: Direct numerical simulations of the network components (U_i, V_i), showing the emergence of a complex locked pattern. The black curve is the unstable synchronous orbit and coloured dots show a snapshot of solution components for an arbitrary time instant. Right: Representation of the simulations via a plot of $V_i(t)$. Parameters as in Fig. 9.

In the next section we extend the analysis here to treat heterogeneous delays.

4. A nonsmooth Wilson-Cowan network with heterogeneous delays

We now consider a network of N Wilson–Cowan nodes with heterogeneous delays given by

$$\frac{\mathrm{d}}{\mathrm{d}t}u_i(t) = -u_i(t) + H\left(I_u + \sum_{j=1}^{N} \mathcal{W}^{uu}_{ij} u_j(t-\tau_{ij}) - \sum_{j=1}^{N} \mathcal{W}^{vu}_{ij} v_j(t-\tau_{ij})\right), \tag{44}$$

$$\kappa\frac{\mathrm{d}}{\mathrm{d}t}v_i(t) = -v_i(t) + H\left(I_v + \sum_{j=1}^{N} \mathcal{W}^{uv}_{ij} u_j(t-\tau_{ij}) - \sum_{j=1}^{N} \mathcal{W}^{vv}_{ij} v_j(t-\tau_{ij})\right), \qquad i = 1,\dots,N. \tag{45}$$

Unlike the generalisation of results from a single node to a network with homogeneous delays, we shall see here that the treatment of heterogeneous delays is more involved and requires some new ideas. Indeed, even for smooth systems the treatment of systems with multiple (and many) delays is not well developed, though see [42, 43] for some restricted applications, and Szalai and Orosz [44] and Otto et al. [45] for more general treatments based on an adjacency lag operator that describes the topology of the network as well as the corresponding coupling delays. Given the challenge of treating truly heterogeneous delays and with a desire to restrict attention to the most informative cases we once again focus on the synchronous network solution. To facilitate this we consider only ring networks with distance dependent interactions, both in strength and delay. Namely, we choose $\mathcal{W}^{\alpha\beta}_{ij} = w^{\alpha\beta}\epsilon_c^{\mathrm{dist}(i,j)}$ and $\tau_{ij} = \tau + \mathrm{dist}(i,j)\epsilon_d$, and an odd number of nodes $N = 2M+1$, for $M \in \mathbb{N}_0$. Here, ϵ_c and ϵ_d are used to determine distance dependent coupling strengths and delays, respectively and τ is a fixed common delay. The assumption that communication time delays increase with distance is a natural one, and for further simplicity we shall restrict attention to the case that ϵ_d is such that $\max\{\tau_{ij}\}$ is less than any time-of-flight for a trajectory between switches.

Substituting a synchronous solution of the form $(u_i(t), v_i(t)) = (\overline{u}(t), \overline{v}(t))$, for all $i = 1,\dots,N$, into the ring network version of (44)-(45), shows that, if it exists, then a synchronous network state is a periodic solution of

$$\frac{\mathrm{d}}{\mathrm{d}t}\overline{u}(t) = -\overline{u}(t) + H\left(I_u + \sum_{m=0}^{M} \sigma_{0,m}\left(w^{uu}\overline{u}(t-\tau_m) - w^{vu}\overline{v}(t-\tau_m)\right)\right), \tag{46}$$

$$\kappa\frac{\mathrm{d}}{\mathrm{d}t}\overline{v}(t) = -\overline{v}(t) + H\left(I_v + \sum_{m=0}^{M} \sigma_{0,m}\left(w^{uv}\overline{u}(t-\tau_m) - w^{vv}\overline{v}(t-\tau_m)\right)\right), \tag{47}$$

where

$$\sigma_{0,m} = (2-\delta_{0,m})\epsilon_c^m, \qquad \tau_m = \tau + m\epsilon_d, \tag{48}$$

and $\delta_{n,m}$ is a Kronecker delta function. Given the potentially large numbers of delays in (46)-(47), the Fourier series approach developed in section 2.1 is an efficient way to construct a periodic solution and we adopt this approach here. For ease of exposition we denote arguments of functions H in (46) and (47) by $\chi_{\overline{u}}(t)$ and $\chi_{\overline{v}}(t)$ respectively, Then we denote unknown times-of-flight of the orbit by: T_1 in the region $\chi_{\overline{u}} > 0$ and $\chi_{\overline{v}} > 0$, T_2 in the region $\chi_{\overline{u}} < 0$ and $\chi_{\overline{v}} > 0$, T_3 in the region $\chi_{\overline{u}} < 0$ and $\chi_{\overline{v}} < 0$, and T_4 in the region $\chi_{\overline{u}} > 0$ and $\chi_{\overline{v}} < 0$. The period of the orbit is $\Delta = \sum_{i=1}^{4} T_i$. By following the method shown in section 2.1 we can compute Fourier coefficients of Δ-periodic solutions in terms of the unknown time of flights, and then determine these self-consistently. See Appendix B for explicit formulas. An illustration of an orbit constructed in this way is given

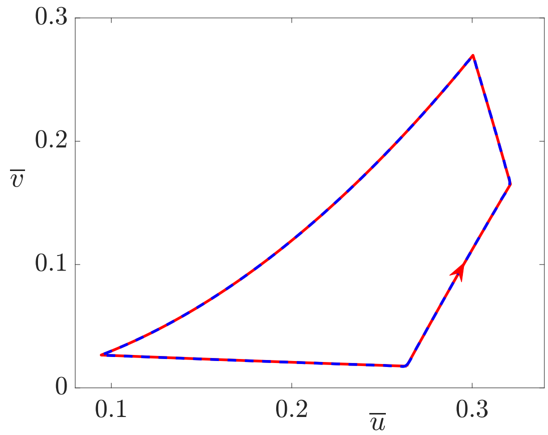

Figure 11: A synchronous periodic orbit constructed for a Wilson–Cowan ring network with distance dependent interactions. The Fourier approach is used to construct the orbit depicted in dashed blue, and the less computationally efficient matrix exponential method in red. Parameters: $\kappa = 0.5$, $I_u = -0.05$, $I_v = -0.3$, $w^{uu} = 1$, $w^{vu} = 2$, $w^{uv} = 1$, $w^{vv} = 0.25$, $\tau = 0.018$, $\epsilon_d = 0.002$, and $\epsilon_c = 0.1$.

in Fig. 11 (which also shows the same orbit constructed with the computationally less efficient matrix exponential approach).

In order to analyse stability of synchronous orbit let us consider perturbed solutions in the form $(u_i(t), v_i(t)) = (\overline{u}(t) + \delta u_i(t), \overline{v}(t) + \delta v_i(t))$. Then perturbations evolve according to

$$\frac{\mathrm{d}}{\mathrm{d}t}\delta u_i(t) = -\delta u_i(t) + \delta(\chi_{\overline{u}})\left(\sum_{j=1}^{N} \mathcal{W}^{uu}_{ij}\delta u_j(t-\tau_{ij}) - \sum_{j=1}^{N} \mathcal{W}^{vu}_{ij}\delta v_j(t-\tau_{ij})\right), \tag{49}$$

$$\kappa\frac{\mathrm{d}}{\mathrm{d}t}\delta v_i(t) = -\delta v_i(t) + \delta(\chi_{\overline{v}})\left(\sum_{j=1}^{N} \mathcal{W}^{uv}_{ij}\delta u_j(t-\tau_{ij}) - \sum_{j=1}^{N} \mathcal{W}^{vv}_{ij}\delta v_j(t-\tau_{ij})\right), \tag{50}$$

where $\delta(\chi_{\overline{u}})$ and $\delta(\chi_{\overline{v}})$ are Dirac delta functions. Here for $m = 0, \ldots, M$, we introduce a 2×2 block notation using:

$$\widetilde{W}_m = \begin{bmatrix} \delta(\chi_{\overline{u}})\mathcal{W}^{uu}_m & -\delta(\chi_{\overline{u}})\mathcal{W}^{vu}_m \\ \delta(\chi_{\overline{v}})\mathcal{W}^{uv}_m & -\delta(\chi_{\overline{v}})\mathcal{W}^{vv}_m \end{bmatrix}. \tag{51}$$

We can then rewrite (49)-(50) in the vector form for $i = 1, \ldots, N$ as:

$$
\begin{aligned}
\frac{\mathrm{d}}{\mathrm{d}t}\begin{bmatrix} \delta u_1(t) \\ \kappa\delta v_1(t) \\ \vdots \\ \delta u_N(t) \\ \kappa\delta v_N(t) \end{bmatrix} &= -\begin{bmatrix} \delta u_1(t) \\ \delta v_1(t) \\ \vdots \\ \delta u_N(t) \\ \delta v_N(t) \end{bmatrix} + \begin{bmatrix} \widetilde{W_0} & 0 & 0 & \ldots & 0 \\ 0 & \widetilde{W_0} & 0 & \ldots & 0 \\ \vdots & \ldots & \ddots & \ldots & \vdots \\ 0 & 0 & \ldots & \widetilde{W_0} & 0 \\ 0 & \ldots & 0 & 0 & \widetilde{W_0} \end{bmatrix}\begin{bmatrix} \delta u_1(t-\tau_0) \\ \delta v_1(t-\tau_0) \\ \vdots \\ \delta u_N(t-\tau_0) \\ \delta v_N(t-\tau_0) \end{bmatrix} \\
&+ \begin{bmatrix} 0 & \widetilde{W_1} & 0 & \ldots & \widetilde{W_1} \\ \widetilde{W_1} & 0 & \widetilde{W_1} & \ldots & 0 \\ \ldots & \ldots & \ldots & \ldots & \ldots \\ 0 & \ldots & \widetilde{W_1} & 0 & \widetilde{W_1} \\ \widetilde{W_1} & \ldots & 0 & \widetilde{W_1} & 0 \end{bmatrix}\begin{bmatrix} \delta u_1(t-\tau_1) \\ \delta v_1(t-\tau_1) \\ \vdots \\ \delta u_N(t-\tau_1) \\ \delta v_N(t-\tau_1) \end{bmatrix} + \ldots \\
&+ \begin{bmatrix} 0 & \ldots & 0 & \widetilde{W_M} & \widetilde{W_M} & 0 & 0 & \ldots & 0 \\ 0 & \ldots & 0 & 0 & \widetilde{W_M} & \widetilde{W_M} & 0 & \ldots & 0 \\ \ldots & \ldots & \ldots & \ldots & \ldots & \ldots & \ldots & \ldots & \ldots \\ \widetilde{W_M} & \widetilde{W_M} & 0 & \ldots & \ldots & \ldots & \ldots & \ldots & 0 \\ \ldots & \ldots & \ldots & \ldots & \ldots & \ldots & \ldots & \ldots & \ldots \\ 0 & \ldots & \widetilde{W_M} & \widetilde{W_M} & 0 & \ldots & 0 & 0 & 0 \end{bmatrix}\begin{bmatrix} \delta u_1(t-\tau_M) \\ \delta v_1(t-\tau_M) \\ \vdots \\ \delta u_N(t-\tau_M) \\ \delta v_N(t-\tau_M) \end{bmatrix}.
\end{aligned} \tag{52}
$$

Then using the coupling strength definition $\mathcal{W}_m^{\alpha\beta} = w^{\alpha\beta}\epsilon_c^m$, we obtain the relation $\widetilde{W}_m = \epsilon_c^m \widetilde{W}$, with

$$
\widetilde{W} = \begin{bmatrix} \delta(\chi_{\overline{u}})w^{uu} & -\delta(\chi_{\overline{u}})w^{vu} \\ \delta(\chi_{\overline{v}})w^{uv} & -\delta(\chi_{\overline{v}})w^{vv} \end{bmatrix}. \tag{53}
$$

Using the above notation we can write the above in a more compact form. First we introduce a vector notation with $Y = (u_1, v_1, u_2, v_2, \ldots, u_N, v_N) \in \mathbb{R}^{2N}$. If we denote the synchronous solution by $\overline{Y}(t) = (\overline{u}(t), \overline{v}(t), \overline{u}(t), \overline{v}(t), \ldots, \overline{u}(t), \overline{v}(t))$ and consider small perturbations such that $Y = \overline{Y} + \delta Y$, then (52) can be written in the vector notation

$$
\frac{\mathrm{d}}{\mathrm{d}t}\delta Y(t) = (I_N \otimes \overline{A})\delta Y(t) + \sum_{m=0}^{M}(A_m \otimes J\widetilde{W})\delta Y(t-\tau_m), \tag{54}
$$

where $\overline{A} = -J$ (J is given in (3)) and A_m are circulant matrices produced by using vectors of the form

$$
\epsilon_c^m(a_0, a_1, \ldots, a_m, \ldots, a_{N-m}, \ldots, a_{N-1}), \tag{55}
$$

such that entries $a_m = a_{N-m} = 1$ and the other entries are zero (they only take the value 1 at the m^{th} and $N - m^{th}$ entries and the rest are zero). Some examples of A_m are

$$
A_0 = \mathrm{Circulant}([\epsilon_c^0, 0, \ldots, 0]) \equiv \epsilon_c^0 I_N, \tag{56}
$$

$$
A_1 = \mathrm{Circulant}([0, \epsilon_c^1, 0, \ldots, 0, \epsilon_c^1]), \tag{57}
$$

$$
A_2 = \mathrm{Circulant}([0, 0, \epsilon_c^2, 0 \ldots, 0, \epsilon_c^2, 0]). \tag{58}
$$

It is now convenient to introduce the lag operator $\mathcal{L}(\tau)$ [44, 45] defined by

$$
\mathcal{L}(\tau)y(t) = y(t-\tau), \tag{59}
$$

and write the linearized dynamics (54) as

$$\frac{\mathrm{d}}{\mathrm{d}t}\delta Y(t) = \left[I_N \otimes \overline{A} + \mathcal{B} \otimes J\widetilde{W}\right]\delta Y(t), \tag{60}$$

where the so-called *adjacency lag operator* $\mathcal{B}$ is defined by

$$\mathcal{B} = \sum_{m=0}^{M} A_m \mathcal{L}(\tau_m). \tag{61}$$

The adjacency lag operator contains all the information about the network topology (given by the matrices A_m) and the coupling delays (specified by the lag operators $\mathcal{L}(\tau_m)$). Since the circulant matrices A_m share the same eigenvectors, the 'eigenvalues' of $\mathcal{B}$ are operators D_q, given by

$$D_q = \sum_{m=0}^{M} \sigma_{q,m} \mathcal{L}(\tau_m), \tag{62}$$

where $\sigma_{q,m}$ are the eigenvalues of the matrices A_m belonging to the eigenvector $e_q = (1, \omega_q, \omega_q^2, \ldots, \omega_q^{N-1})/\sqrt{N}$, where $q = 0, \ldots, N-1$, and $\omega_q = \exp(2\pi \mathrm{i} q/N)$ are the Nth roots of unity. Hence, the operators D_q are linear combination of the lag operators. Note that we may construct the values $\sigma_{q,m}$ from the elements of the row generator of the circulant matrix A_m, denoted by A_m^j for $j = 0, \ldots, N-1$, as $\sigma_{q,m} = \sum_{j=0}^{N-1} A_m^j \omega_q^j$.

If we introduce the matrix of eigenvectors $P = [e_0 \; e_1 \; \ldots \; e_{N-1}]$, then we have that

$$P^{-1}\mathcal{B}P = \mathrm{diag}(D_0, D_1, \ldots, D_{N-1}) \equiv \Lambda. \tag{63}$$

Using a change of variable $\delta Z = (P \otimes I_2)^{-1}\delta Y$ and applying $(P \otimes I_2)^{-1}$ to the both sides of the system (60) we obtain

$$\frac{\mathrm{d}}{\mathrm{d}t}\delta Z(t) = (I_N \otimes \overline{A})\delta Z(t) + (\Lambda \otimes J\widetilde{W})\delta Z(t). \tag{64}$$

This has a 2×2, $N-$block structure with the dynamics in each block given by

$$\frac{\mathrm{d}}{\mathrm{d}t}\xi_q(t) = \left[\overline{A} + J\widetilde{W}D_q\right]\xi_q(t), \quad q = 0, \ldots, N-1, \quad \xi_q \in \mathbb{C}^2. \tag{65}$$

Thus to determine the stability of the synchronous state we only have to consider a set of N two dimensional variational problems. Each of these can be solved using the method described in Section 3. That is between the events we have $\widetilde{W} = 0$ and system evolves according to $\xi_q' = \overline{A}\xi_q$. Moreover across the switching times we have

$$\xi_q(\Delta_j^+) = \xi_q(\Delta_j^-) + K_j \sum_{m=0}^{M} \sigma_{q,m}\xi_q(\Delta_j - \tau_m), \tag{66}$$

where

$$K_1 = \frac{1}{\chi_{\overline{u}}'(\Delta_1)} J \begin{bmatrix} 1 & 0 \\ 0 & 0 \end{bmatrix} W, \qquad K_2 = \frac{-1}{\chi_{\overline{v}}'(\Delta_2)} \begin{bmatrix} 0 & 0 \\ 0 & 1 \end{bmatrix} W,$$

$$K_3 = \frac{-1}{\chi_{\overline{u}}'(\Delta_3)} J \begin{bmatrix} 1 & 0 \\ 0 & 0 \end{bmatrix} W, \qquad K_4 = \frac{1}{\chi_{\overline{v}}'(\Delta_4)} J \begin{bmatrix} 0 & 0 \\ 0 & 1 \end{bmatrix} W. \tag{67}$$

Here we have

$$\chi'_{\overline{u}}(t) = \sum_{m=0}^{M} \sigma_{0,m}(w^{uu}\overline{u}'(t-\tau_m) - w^{vu}\overline{v}'(t-\tau_m)), \tag{68}$$

$$\chi'_{\overline{v}}(t) = \sum_{m=0}^{M} \sigma_{0,m}(w^{uv}\overline{u}'(t-\tau_m) - w^{vv}\overline{v}'(t-\tau_m)). \tag{69}$$

The formulation above now puts us in an ideal situation to develop the relevant Floquet theory by using exactly those techniques developed in section 3. Namely, we write $\xi_q(t) = \mathrm{e}^{\lambda t} z_q(t)$, for $\lambda \in \mathbb{C}$ (Floquet exponents) with $z_q(t)$ a Δ−periodic function. Then away from switches these evolve according to $z'_q = \left(\overline{A} - \lambda I_2\right) z'_q$ and across switching events, we have

$$z_q(\Delta_j^+) = z_q(\Delta_j^-) + K_j \sum_{m=0}^{M} \sigma_{q,m} \mathrm{e}^{-\lambda\tau_m} z_q(\Delta_j - \tau_m). \tag{70}$$

To compute $z_q(t)$ on $[0, \Delta]$ we can proceed analogously to the formulation of (20). However, we now have to determine the amplitude of z_q at a larger set of $4(M+1)$ times given by $t = \Delta_i - \tau_m$ for $i = 1, \ldots, 4$ and $m = 0, \ldots, M$. Following the earlier self-consistent approach, as described in section 2.2, the Floquet exponents can be found as the zeros of a complex function $\mathcal{E}_q(\lambda) \equiv \det(\mathscr{U}_q(\lambda)) = 0$, where $\mathscr{U}_q(\lambda)$ has the block form

$$\mathscr{U}_q(\lambda) = \begin{bmatrix} G_1(\Delta_1, \lambda, q) & G_2(\Delta_1, \lambda, q) & G_3(\Delta_1, \lambda, q) & G_4(\Delta_1, \lambda, q) \\ F_1(\Delta_2, \lambda, q) & G_5(\Delta_2, \lambda, q) & G_3(\Delta_2, \lambda, q) & G_4(\Delta_2, \lambda, q) \\ F_1(\Delta_3, \lambda, q) & F_2(\Delta_3, \lambda, q) & G_6(\Delta_3, \lambda, q) & G_4(\Delta_3, \lambda, q) \\ F_1(\Delta_4, \lambda, q) & F_2(\Delta_4, \lambda, q) & F_3(\Delta_4, \lambda, q) & G_7(\Delta_4, \lambda, q) \end{bmatrix}. \tag{71}$$

The detailed forms of the block entries of $\mathscr{U}_q(\lambda)$ are given in Appendix C. The synchronous network state will be linearly stable provided all solutions of $\mathcal{E}_q(\lambda) = 0$ have $\operatorname{Re}\lambda < 0$ for all $q = 0, \ldots, N-1$ (excluding a parameter independent zero eigenvalue arising from time-translation invariance).

4.1. Instabilities in a ring network: heterogeneous delays

Similarly to the presentation in section 3.1 we now illustrate the theory developed above for heterogeneous delays with some direct numerical simulations, as well as the determination of

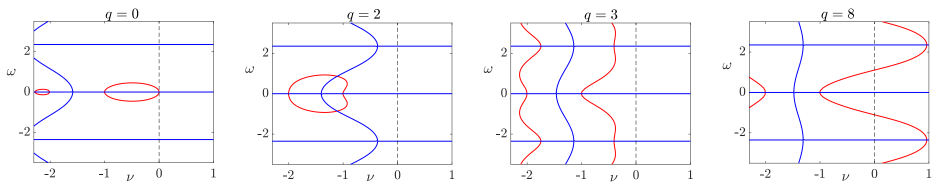

Figure 12: The Floquet exponents for a Wilson–Cowan ring network with $N = 31$ nodes and heterogeneous delays (as intersections of the zero contours of $\mathcal{E}_q^{\mathrm{I,R}}(\lambda)$, given by the red and blue lines). Here we see that the mode with $q = 8$ is unstable (and for this example many other modes are also unstable). Parameters: $\mu = 0.45$, $\tau = 0.02$, $\epsilon_d = 0.00295$, and other parameters as in Fig. 11.

Floquet exponents using numerical plots like that of Fig. 12. We adopt the same coupling matrix as in (43) by choosing

$$\epsilon_c^{\mathrm{dist}(i,j)} = \frac{\mathrm{e}^{-\mathrm{dist}(i,j)/\mu}}{\sum_{j=0}^{N-1} \mathrm{e}^{-\mathrm{dist}(0,j)/\mu}}, \tag{72}$$

with $\mathcal{W}_{ij}^{\alpha\beta} = w^{\alpha\beta}\epsilon_c^{\mathrm{dist}(i,j)}$. For small values of ϵ_d, remembering that $\tau_{ij} = \tau + \mathrm{dist}(i,j)\epsilon_d$, then we expect to uncover similar behaviour as for the case of homogeneous delays (recovered with $\epsilon_d = 0$). Indeed, in this limit, bifurcation points (for the synchronous network state) are very close to that of the homogeneous delay case, and simulations of behaviours far from bifurcation are also similar. However, when we introduce more heterogeneity to the system by increasing ϵ_d, the network bifurcation point can shift somewhat. For example, when using μ as a bifurcation parameter this can lower the value of μ_c to decrease the overall window of μ where synchrony is stable. This is consistent with the behaviour of networks built from smooth systems with multiple delays [46, 47]. Moreover, and as expected (for a supercritical bifurcation) the unstable eigenvector at the bifurcation point is a good predictor of the emergent network pattern. Further from the bifurcation point (where the linear predictions break down) we find that, in comparison to the case with homogeneous delays, the emergent network dynamics becomes far more irregular with an increase in ϵ_d. We observe that synchronous network activity can destabilise to phase-locked or cluster-like solutions, as well as seemingly chaotic behaviour (not observed with $\epsilon_d = 0$). Examples of such behaviour are shown in Fig. 13. Moreover, qualitatively similar behaviour is found in simulations where the Heaviside firing rate is replaced by a smooth sigmoidal of the type described in section 2 in the high gain limit (large β).

5. Discussion

The study of networks is a relatively new branch of applied nonlinear dynamics. Techniques for the structural and functional analysis of networks include empirical methods, analysis, computer simulation, and graph theory. Although many insights have now been obtained about the behaviour of particular types of network solutions [48], and perhaps most notably the stability of synchrony in networks of identical modes with graph Laplacian structural interactions using the master stability function approach [49], it is fair to say that corresponding results for delayed interactions are far fewer. Given that this is one of the defining features for a white matter brain network, with synaptic interactions mediated by the propagation of finite speed action potentials, there is a pressing need for the development of theoretical approaches in this area to help understand how patterns of functional connectivity, so readily observed in neuroimaging studies, emerge from an interplay of local dynamics, axonal wiring, and the resultant delayed interactions arising from communication along white matter fibre tracts.

In this paper, we have developed a set of mathematical tools to study the nonsmooth Wilson–Cowan neural population activity model with delay terms at both the node and network level. We began by showing how to construct a delay induced periodic orbit in a single node as well as describing how to determine stability by augmenting Floquet theory for smooth systems with saltation operators to cope with the evolution of jumps in the linearised equations. We bootstrapped this approach, first to a ring network with a single homogeneous delay, and then to one with distance-dependent heterogeneous delays. The latter analysis making use of an adjacency lag operator, encoding the network topology and delay structure [44, 45], to best express the linearised equations for determining the stability of the synchronous state. The resulting framework

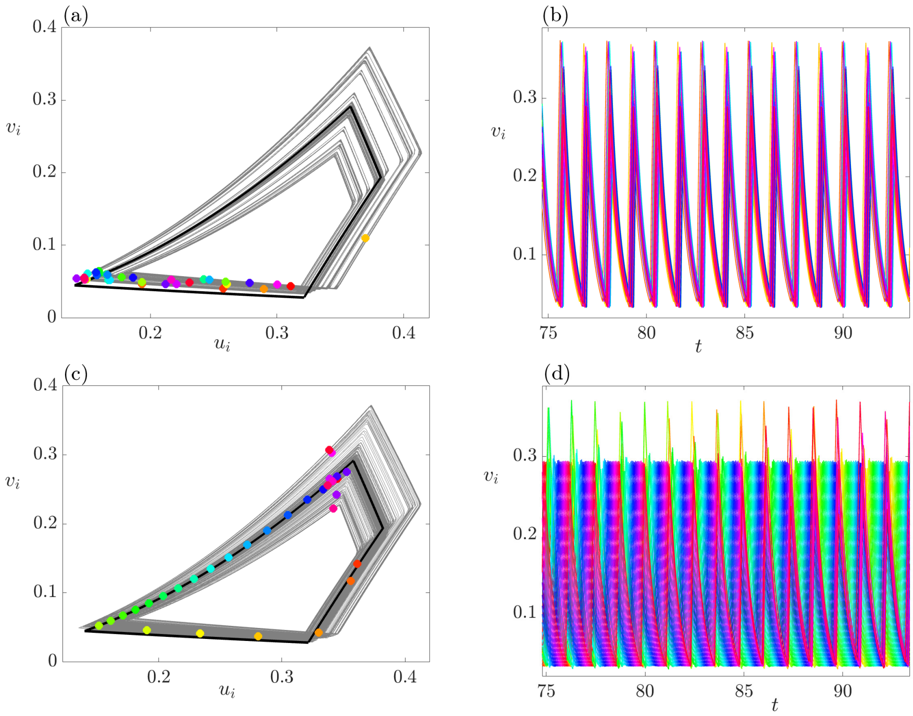

Figure 13: Dynamics of a Wilson–Cowan ring network with $N = 31$ nodes and heterogeneous delays in parameter regimes where the synchronous network state is linearly unstable. Here, $\epsilon_d = 0.0028$ for (a,b) and $\epsilon_d = 0.00295$ for (c,d). Other parameters as in Fig. 12. (a,c): Direct numerical simulations of the network components (u_i, v_i). The black curve is the unstable synchronous orbit and coloured dots show a snapshot of system states at a fixed time instant. (b,d): Representation of the simulations via a plot of $v_i(t)$ (with the same colouring as in the left panels). As ϵ_d increases more irregular solutions are obtained.

was used to predict the onset of spatio-temporal patterning via an instability of the synchronous network state and confirmed against direct numerical simulations.

A number of natural extensions of the work presented here are possible. One is to extend the analysis to non-synchronous states, such as phase-locked ones with a constant phase lag between each pair of oscillatory nodes. Another would be to probe the phenomenon of *complexity collapse*, whereby the effect of multiple delays in a high-dimensional chaotic neural network can actually leads to a reduction in dynamical complexity [50]. Yet another is to address structural networks and their concomitant delays as recorded in the Human Connectome Project for human brains [51]. Moving beyond the assumption of identical nodes is a further worthy challenge, as too is the consideration of excitable, rather than oscillatory, nodes. Indeed, the study of large scale brain network models with delays is still in its infancy, at least with respect to theoretical investigations, although those based upon computational approaches (including with more sophisticated neural mass models) are progressing rapidly, as exemplified by [52]. However, before pursuing these important extensions it is well to mention that white matter is now known to be *plastic*, see e.g., [53, 54, 55]. This has recently begun to be explored from a modelling perspective by Lefebvre and colleagues [56, 57, 58, 59], with recent work by Fields and colleagues emphasising the role of oligodendrocyte-mediated myelin plasticity in facilitating neural synchronisation [60, 61]. In future work we plan to report on the extension of the analysis presented here to model activity dependent myelination and develop the mathematical analysis of neural mass networks with state-dependent delays.

6. Acknowledgements

This work was supported by the Engineering and Physical Sciences Research Council [grant number EP/V04866X/1].

Appendix A. Saltation operators

The saltation operators given by (17) and (18) described in section 2.2 can be given in an explicit form at the crossing times. We know that at $t = \Delta_1$ and $t = \Delta_3$, we have $\overline{V}(\Delta_1 - \tau) = 0$ and $\overline{V}(\Delta_3 - \tau) = 0$, and also at $t = \Delta_2$ and $t = \Delta_4$, we have $\overline{U}(\Delta_2 - \tau) = 0$ and $\overline{U}(\Delta_4 - \tau) = 0$, respectively. Therefore we need to compute four saltation matrices for these four event times. As an example let us consider at $t = \Delta_1$, where we have from (17) that

$$K_1 = \frac{1}{\overline{V}'(\Delta_1^- - \tau)} \begin{bmatrix} 0 & \overline{U}'(\Delta_1^+) - \overline{U}'(\Delta_1^-) \\ 0 & \overline{V}'(\Delta_1^+) - \overline{V}'(\Delta_1^-) \end{bmatrix}. \tag{A.1}$$

At $t = \Delta_1$, we can use equation (4) to compute derivatives $\overline{U}'$, $\overline{V}'$ in (A.1), and hence we obtain

$$\begin{bmatrix} \overline{U}'(\Delta_1^+) \\ \overline{V}'(\Delta_1^+) \end{bmatrix} - \begin{bmatrix} \overline{U}'(\Delta_1^-) \\ \overline{V}'(\Delta_1^-) \end{bmatrix} = WJ \left(\begin{bmatrix} 1 \\ 1 \end{bmatrix} - \begin{bmatrix} 1 \\ 0 \end{bmatrix} \right) = \begin{bmatrix} -w^{vu}/\kappa \\ -w^{ww}/\kappa \end{bmatrix}. \tag{A.2}$$

Using (A.1), (A.2), and W, J in (3), we find

$$K_1 = \frac{1}{\overline{V}'(\Delta_1^- - \tau)} \begin{bmatrix} 0 & -w^{vu}/\kappa \\ 0 & -w^{ww}/\kappa \end{bmatrix} = \frac{1}{\overline{V}'(\Delta_1^- - \tau)} WJ \begin{bmatrix} 0 & 0 \\ 0 & 1 \end{bmatrix}, \tag{A.3}$$

Similarly we compute all saltation operators for each $t = \Delta_j$, $j = 1, \ldots, 4$, to yield (19).

Appendix B. Fourier approach for calculating the periodic orbit of a system with heterogenous delays

Consider the equations given by (46)-(47). The zeros of the arguments to the Heaviside functions H in these equations define the switching times. Adopting a Fourier series representation $(\overline{u}(t), \overline{v}(t)) = \sum_{n\in\mathbb{Z}} (u_n, v_n) \mathrm{e}^{2\pi \mathrm{i} nt/\Delta}$ then the four switching conditions for the four unknowns Δ_i, $i = 1, \ldots, 4$ can be written

$$I_u + \sum_{m=0}^{M} \sigma_{0,m} \left(w^{uu} \sum_n u_n \mathrm{e}^{\frac{2\pi i n(\Delta_1 - \tau_m)}{\Delta}} - w^{vu} \sum_n v_n \mathrm{e}^{\frac{2\pi i n(\Delta_1 - \tau_m)}{\Delta}} \right) = 0, \tag{B.1}$$

$$I_v + \sum_{m=0}^{M} \sigma_{0,m} \left(w^{uv} \sum_n u_n \mathrm{e}^{\frac{2\pi i n(\Delta_2 - \tau_m)}{\Delta}} - w^{vv} \sum_n v_n \mathrm{e}^{\frac{2\pi i n(\Delta_2 - \tau_m)}{\Delta}} \right) = 0, \tag{B.2}$$

$$I_u + \sum_{m=1}^{M} \sigma_{0,m} \left(w^{uu} \sum_n u_n \mathrm{e}^{\frac{2\pi i n(\Delta_3 - \tau_m)}{\Delta}} - w^{vu} \sum_n v_n \mathrm{e}^{\frac{2\pi i n(\Delta_3 - \tau_m)}{\Delta}} \right) = 0, \tag{B.3}$$

$$I_v + \sum_{m=1}^{M} \sigma_{0,m} \left(w^{uv} \sum_n u_n \mathrm{e}^{\frac{2\pi i n(\Delta - \tau_m)}{\Delta}} - w^{vv} \sum_n v_n \mathrm{e}^{\frac{2\pi i n(\Delta - \tau_m)}{\Delta}} \right) = 0. \tag{B.4}$$

The coefficients (u_n, v_n), in terms of $(\Delta_1, \Delta_2, \Delta_3, \Delta_4)$ are given by (9). The simultaneous (numerical) solution of the four equations above determines the set $(\Delta_1, \Delta_2, \Delta_3, \Delta_4)$.

Appendix C. Block entries

The block entries of (71) have the explicit forms:

$$[G_1(t,\lambda,q)]_{ij} = g_1(t-\tau_{i-1})\sigma_{q,j-1}\mathrm{e}^{-\lambda\tau_{j-1}} - [I_{2(M+1)}]_{ij}, \tag{C.1}$$
$$[G_2(t,\lambda,q)]_{ij} = g_2(t-\tau_{i-1})\sigma_{q,j-1}\mathrm{e}^{-\lambda\tau_{j-1}}, \tag{C.2}$$
$$[G_3(t,\lambda,q)]_{ij} = g_3(t-\tau_{i-1})\sigma_{q,j-1}\mathrm{e}^{-\lambda\tau_{j-1}}, \tag{C.3}$$
$$[G_4(t,\lambda,q)]_{ij} = g_4(t-\tau_{i-1})\sigma_{q,j-1}\mathrm{e}^{-\lambda\tau_{j-1}}, \tag{C.4}$$
$$[G_5(t,\lambda,q)]_{ij} = g_2(t-\tau_{i-1})\sigma_{q,j-1}\mathrm{e}^{-\lambda\tau_{j-1}} - [I_{2(M+1)}]_{ij}, \tag{C.5}$$
$$[G_6(t,\lambda,q)]_{ij} = g_3(t-\tau_{i-1})\sigma_{q,j-1}\mathrm{e}^{-\lambda\tau_{j-1}} - [I_{2(M+1)}]_{ij}, \tag{C.6}$$
$$[G_7(t,\lambda,q)]_{ij} = g_4(t-\tau_{i-1})\sigma_{q,j-1}\mathrm{e}^{-\lambda\tau_{j-1}} - [I_{2(M+1)}]_{ij}, \tag{C.7}$$
$$[F_1(t,\lambda,q)]_{ij} = f_1(t-\tau_{i-1})\sigma_{q,j-1}\mathrm{e}^{-\lambda\tau_{j-1}}, \tag{C.8}$$
$$[F_2(t,\lambda,q)]_{ij} = f_2(t-\tau_{i-1})\sigma_{q,j-1}\mathrm{e}^{-\lambda\tau_{j-1}}, \tag{C.9}$$
$$[F_3(t,\lambda,q)]_{ij} = f_3(t-\tau_{i-1})\sigma_{q,j-1}\mathrm{e}^{-\lambda\tau_{j-1}}, \tag{C.10}$$

where $i, j = 1,\dots,M+1$, $g_1(t) = \rho(t)\zeta(\Delta-\Delta_1)K_1$, $g_2(t) = \rho(t)\zeta(\Delta-\Delta_2)K_2$, $g_3(t) = \rho(t)\zeta(\Delta-\Delta_3)K_3$, $g_4(t) = \rho(t)K_4$, $f_1(t) = \rho(t)[\rho(\Delta_1)^{-1} + \zeta(\Delta-\Delta_1)]K_1$, $f_2(t) = \rho(t)[\rho(\Delta_2)^{-1} + \zeta(\Delta-\Delta_2)]K_2$, $f_3(t) = \rho(t)[\rho(\Delta_3)^{-1} + \zeta(\Delta-\Delta_3)]K_3$, $\rho(t) = \zeta(t)[I_2 - \zeta(\Delta)]^{-1}$, and $\zeta(t) = \mathrm{e}^{(\overline{A}-\lambda I_2)t}H(t)$.

References

[1] P. L. Nunez, R. Srinivasan, Neocortical dynamics due to axon propagation delays in cortico-cortical fibers: EEG traveling and standing waves with implications for top-down influences on local networks and white matter disease, Brain Research 1542 (2014) 138–166.

[2] S. N. Sotiropoulos, S. Jbabdi, J. Xu, J. L. Andersson, S. Moeller, E. J. Auerbach, M. F. Glasser, M. Hernandez, G. Sapiro, M. Jenkinson, D. A. Feinberg, E. Yacoub, C. Lenglet, D. C. V. Essen, K. Ugurbil, T. E. B. for the WU-Minn HCP Consortium, Advances in diffusion MRI acquisition and processing in the Human Connectome Project, NeuroImage 80 (2013) 125–143. Mapping the Connectome.

[3] B. A. E. Hunt, P. K. Tewarie, O. E. Mougin, N. Geades, D. K. Jones, K. D. Singh, P. G. Morris, P. A. Gowland, M. J. Brookes, Relationships between cortical myeloarchitecture and electrophysiological networks, Proceedings of the National Academy of Sciences USA 113 (2016) 13510–13515.

[4] Z. Ma, N. Zhang, Cross-population myelination covariance of human cerebral cortex, Human Brain Mapping 38 (2017) 4730–4743.

[5] M. M. Vandewouw, B. A. Hunt, J. Ziolkowski, M. J. Taylor, The developing relations between networks of cortical myelin and neurophysiological connectivity, NeuroImage 237 (2021) 118142.

[6] W. A. H. Rushton, A theory of the effects of fibre size in medullated nerve, Journal of Physiology 115 (1951) 101–122.

[7] F. Varela, J.-P. Lachaux, E. Rodriguez, J. Martinerie, The brainweb: Phase synchronization and large-scale integration, Nature Reviews Neuroscience 2 (2001) 229–239.

[8] P. J. Uhlhaas, W. Singer, Neural synchrony in brain review disorders: Relevance for cognitive dysfunctions and pathophysiology, Neuron 52 (2006) 155–168.

[9] P. Fries, Neuronal gamma-band synchronization as a fundamental process in cortical computation, Annual Review of Neuroscience 32 (2009) 209–224.

[10] P. Fries, Communication through coherence (CTC 2.0), Neuron 88 (2015) 220–235.

[11] R. Hindriks, M. Woolrich, H. Luckhoo, M. Joensson, H. Mohseni, M. Kringelbach, G. Deco, Role of white-matter pathways in coordinating alpha oscillations in resting visual cortex, NeuroImage 106 (2015) 328–339.

[12] P. L. Nunez, The brain wave equation: A model for the EEG, Mathematical Biosciences 21 (1974) 279–297.

[13] S. Visser, R. Nicks, O. Faugeras, S. Coombes, Standing and travelling waves in a spherical brain model: the Nunez model revisited, Physica D 349 (2017) 27–45.

[14] P. Sanz-Leon, S. A. Knock, A. Spiegler, V. K. Jirsa, Mathematical framework for large-scale brain network modeling in The Virtual Brain, NeuroImage 111 (2015) 385–430.
[15] H. R. Wilson, J. D. Cowan, Excitatory and inhibitory interactions in localized populations of model neurons., Biophysical Journal 12 (1972) 1–24.
[16] G. Deco, V. Jirsa, A. R. McIntosh, O. Sporns, R. Kötter, Key role of coupling, delay, and noise in resting brain fluctuations., Proceedings of the National Academy of Sciences USA 106 (2009) 10302–10307.
[17] J. Cabral, E. Hugues, O. Sporns, G. Deco, Role of local network oscillations in resting-state functional connectivity, NeuroImage 57 (2011) 130–139.
[18] R. C. Budzinski, T. T. Nguyen, G. B. Benigno, J. Đoàn, J. Mináč, T. J. Sejnowski, L. E. Muller, Analytical prediction of specific spatiotemporal patterns in nonlinear oscillator networks with distance-dependent time delays, Physical Review Research 5 (2023) 013159.
[19] R. G. Abeysuriya, J. Hadida, S. N. Sotiropoulos, S. Jbabdi, R. Becker, B. A. E. Hunt, M. J. Brookes, M. W. Woolrich, A biophysical model of dynamic balancing of excitation and inhibition in fast oscillatory large-scale networks, PLOS Computational Biology 14 (2018) e1006007.
[20] N. Williams, A. Ojanperä, F. Siebenhühner, B. Toselli, S. Palva, G. Arnulfo, S. Kaski, J. Palva, The influence of inter-regional delays in generating large-scale brain networks of phase synchronization, bioRxiv (2023).
[21] C. M. Marcus, R. M. Westervelt, Stability of analog neural networks with delay, Physical Review A 39 (1989) 347–359.
[22] P. Baldi, A. F. Atiya, How delays affect neural dynamics and learning, IEEE Transactions on Neural Networks 5 (1994) 612–621.
[23] S. Coombes, C. Laing, Delays in activity-based neural networks, Philosophical Transactions of the Royal Society A 367 (2009) 1117–1129.
[24] P. Tewarie, R. Abeysuriya, Á. Byrne, G. C. O'Neill, S. N. Sotiropoulos, M. J. Brookes, S. Coombes, How do spatially distinct frequency specific meg networks emerge from one underlying structural connectome? the role of the structural eigenmodes, NeuroImage 186 (2019) 211–220.
[25] A. Otto, G. Radons, D. Bachrathy, G. Orosz, Synchronization in networks with heterogeneous coupling delays, Physical Review E 97 (2018) 012311.
[26] S. Coombes, Y. M. Lai, M. Şayli, R. Thul, Networks of piecewise linear neural mass models, European Journal of Applied Mathematics 29 (2018) 869–890.
[27] S. Coombes, C. Laing, Instabilities in threshold-diffusion equations with delay, Physica D 238 (2009) 264–272.
[28] H. R. Wilson, J. D. Cowan, Excitatory and inhibitory interactions in localized populations of model neurons, Biophysical journal 12 (1972) 1–24.
[29] A. Destexhe, T. J. Sejnowski, The Wilson–Cowan model, 36 years later, Biological Cybernetics 101 (2009) 1–2.
[30] J. K. Hale, S. M. V. Lunel, Introduction to functional differential equations, volume 99, Springer Science & Business Media, 2013.
[31] D. A. Barton, B. Krauskopf, R. E. Wilson, Periodic solutions and their bifurcations in a non-smooth second-order delay differential equation, Dynamical Systems 21 (2006) 289–311.
[32] J. Harris, B. Ermentrout, Bifurcations in the Wilson–Cowan equations with nonsmooth firing rate, SIAM Journal on Applied Dynamical Systems 14 (2015) 43–72.
[33] B.-K. Kim, Piecewise linear dynamic systems with time delays, Ph.D. thesis, California Institute of Technology, 1972.
[34] W. Bayer, et al., Oscillation types and bifurcations of a nonlinear second-order differential-difference equation, Journal of Dynamics and Differential Equations 10 (1998) 303–326.
[35] U. an der Heiden, A. Longtin, M. Mackey, J. Milton, R. Scholl, Oscillatory modes in a nonlinear second-order differential equation with delay, Journal of Dynamics and Differential Equations 2 (1990) 423–449.
[36] J. Sieber, Dynamics of delayed relay systems, Nonlinearity 19 (2006) 2489.
[37] R. Edwards, P. Van Den Driessche, L. Wang, Periodicity in piecewise-linear switching networks with delay, Journal of mathematical biology 55 (2007) 271–298.
[38] D. A. Barton, Stability calculations for piecewise-smooth delay equations, International Journal of Bifurcation and Chaos 19 (2009) 639–650.
[39] J. Sieber, P. Kowalczyk, S. Hogan, M. Di Bernardo, Dynamics of symmetric dynamical systems with delayed switching, Journal of Vibration and Control 16 (2010) 1111–1140.
[40] P. Kowalczyk, The dynamics and event-collision bifurcations in switched control systems with delayed switching, Physica D: Nonlinear Phenomena 406 (2020) 132407.
[41] N. J. Kong, J. J. Payne, J. Zhu, A. M. Johnson, Saltation matrices: The essential tool for linearizing hybrid dynamical systems, arXiv preprint arXiv:2306.06862 (2023).
[42] A. Englert, S. Heiligenthal, W. Kinzel, I. Kanter, Synchronization of chaotic networks with time-delayed couplings: An analytic study, Physical Review E 83 (2011) 046222.
[43] O. D'Huys, S. Zeeb, T. Jüngling, S. Heiligenthal, S. Yanchuk, W. Kinzel, Synchronisation and scaling properties

of chaotic networks with multiple delays, EPL (Europhysics Letters) 103 (2013) 10013.
[44] R. Szalai, G. Orosz, Decomposing the dynamics of heterogeneous delayed networks with applications to connected vehicle systems, Physical Review E 88 (2013) 040902.
[45] A. Otto, G. Radons, D. Bachrathy, G. Orosz, Synchronization in networks with heterogeneous coupling delays, Physical Review E 97 (2018) 012311.
[46] I. Al-Darabsah, L. Chen, W. Nicola, S. A. Campbell, The impact of small time delays on the onset of oscillations and synchrony in brain networks, Frontiers in Systems Neuroscience (2021) 58.
[47] I. Al-Darabsah, M. Al Janaideh, S. A. Campbell, Stability of connected autonomous vehicle networks with commensurate time delays, in: 2021 American Control Conference (ACC), IEEE, 2021, pp. 3308–3313.
[48] M. A. Porter, J. P. Gleeson, Dynamical Systems on Networks: A Tutorial, volume 4 of *Frontiers in Applied dynamical Systems: Reviews and Tutorials*, Springer International Publishing, Cham, Switzerland, 2016.
[49] L. M. Pecora, T. L. Carroll, Master stability function for synchronized coupled systems, Physical Review Letters 80 (1998) 2109–2112.
[50] S. K. Tavakoli, A. Longtin, Complexity collapse, fluctuating synchrony, and transient chaos in neural networks with delay clusters, Frontiers in Systems Neuroscience 15 (2021).
[51] D. C. Van Essen, S. M. Smith, D. M. Barch, T. E. J. Behrens, E. Yacoub, K. Ugurbil, for the WU-Minn HCP Consortium, The WU-Minn Human Connectome Project: An overview, NeuroImage 80 (2013) 62–79.
[52] G. Rabuffo, J. Fousek, C. Bernard, V. Jirsa, Neuronal cascades shape whole-brain functional dynamics at rest, eNeuro 8 (2021).
[53] R. D. Fields, White matter in learning, cognition and psychiatric disorders, Trends in neurosciences 31 (2008) 361–370.
[54] E. M. Gibson, D. Purger, C. W. Mount, A. K. Goldstein, G. L. Lin, L. S. Wood, I. Inema, S. E. Miller, G. Bieri, J. B. Zuchero, B. A. Barres, P. J. Woo, H. Vogel, M. Monje, Neuronal activity promotes oligodendrogenesis and adaptive myelination in the mammalian brain, Science 344 (2014) 1252304.
[55] L. de Vivo, M. Bellesi, The role of sleep and wakefulness in myelin plasticity, Glia 67 (2019) 2142–2152.
[56] R. Noori, D. Park, J. D. Griffiths, S. Bells, P. W. Frankland, D. Mabbott, J. Lefebvre, Activity-dependent myelination: A glial mechanism of oscillatory self-organization in large-scale brain networks, Proceedings of the National Academy of Sciences USA 117 (2020) 13227–13237.
[57] S. H. Park, J. Lefebvre, Synchronization and resilience in the Kuramoto white matter network model with adaptive state-dependent delays, The Journal of Mathematical Neuroscience 10 (2020) 16.
[58] A. Talidou, P. W. Frankland, D. Mabbott, J. Lefebvre, Learning to be on time: temporal coordination of neural dynamics by activity-dependent myelination, bioRxiv (2021). doi:10.1101/2021.08.17.456520.
[59] A. Talidou, P. W. Frankland, D. Mabbott, J. Lefebvre, Homeostatic coordination and up-regulation of neural activity by activity-dependent myelination, Nature Computational Science 2 (2022) 665–676.
[60] S. Pajevic, P. J. Basser, R. D. Fields, Role of myelin plasticity in oscillations and synchrony of neuronal activity, Neuroscience 276 (2014) 135–147.
[61] S. Pajevic, D. Plenz, P. J. Basser, R. D. Fields, Oligodendrocyte-mediated myelin plasticity and its role in neural synchronization, eLife 12 (2023) e81982.